Czech Technical University in Prague

Faculty of Electrical Engineering
Department Physics

Sound Source Localization in Enclosures

Doctoral Thesis

Adam Koutný

Prague, August 2017

Ph.D. Programme: Electrical Engineering and Information Technology (P2612)
Branch of study: Acoustics (2609V001)

Supervisor: prof. Ing. Ondřej Jiříček, CSc.
Supervisor-Specialist: Ing. Marek Brothánek, Ph. D.

Dissertation Thesis

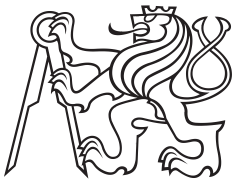

Czech Technical University in Prague

F3

Faculty of Electrical Engineering
Department of Physics

Sound Source Localization in Enclosures

Adam Koutný

Supervisor: prof. Ing. Ondřej Jiříček, CSc.
Supervisor–specialist: Ing. Marek Brothánek, Ph.D.
Field of study: Acoustics (2609V001)
August 2017

Acknowledgements

I would like to thank my supervisors Ondřej Jiříček, Marek Brothánek and Jean-Hugh Thomas for their expert advices and their support during my studies. Also, I would like to thank my colleagues Petr Švec and Vojtěch Jandák for their kind help any time I needed. Last but not least I thanks my wife, family and close friends for patience.

Declaration

I hereby declare that this thesis has been composed by myself and that all sources used have been stated in the thesis bibliography.

In Prague, 30. August 2017

Abstract

This thesis deals with sound source(s) localization and sound field mapping. After a brief overview of common approaches and methods, the thesis focuses specifically on the nearfield acoustical holography. This very promising method provides complete information (amplitude and phase) about the sound field. In comparison to classical and commonly used methods – such as sound power mapping using the intensity probe or sound source(s) localization using the beamforming methods – the nearfield acoustical holography enables three-dimensional sound field description based on the measurement on certain surface. Moreover, through capturing the evanescent waves (present only in the near-field of a source) and their reconstruction, this method provides considerably higher spatial resolution. A mathematical basis of sound radiation – the Helmholtz integral equation and the first and second Rayleigh integral equations – is stated in this thesis. The level of description should provide insight into the method region of validity. The nearfield acoustical holography is based on the inversion of the above mentioned equations describing sound radiation and represents an inverse acoustic problem. Basic regularization techniques are mentioned in this thesis since a correct solution of inverse problems requires transfer functions (matrix) regularization. A description of the Fourier-based nearfield acoustical holography is stated for the planar and spherical coordinate systems, followed by a description of two methods based on the least squares minimization. The results of model simulations as well as real measurement experiments are presented in the practical part of the thesis.

Keywords: acoustics, nearfield acoustical holography, sound field

Supervisor:
prof. Ing. Ondřej Jiříček, CSc.
CTU in Prague,
Faculty of Electrical Engineering,
Department of Physics,
Technická 2,
Praha 6

Supervisor–specialist:
Ing. Marek Brothánek, Ph.D.
CTU in Prague,
Faculty of Electrical Engineering,
Department of Physics,
Technická 2,
Praha 6

Abstrakt

Tato práce se zabývá lokalizací zdrojů zvuku a mapováním zvukových polí. Po krátkém přehledu známých přístupů a metod je práce zaměřena výhradně na akustickou holografii v blízkém poli. Tato metoda má velký potenciál plynoucí ze způsobu měření akustického pole poskytujícího úplnou informaci (amplitudu i fázi) vhodnou pro další zpracování. Ve srovnání s klasickými a běžně používanými metodami – jako mapování vyzářeného akustického výkonu pomocí intenzitní sondy nebo lokalizací zdrojů zvuku metodami *beamformingu* – umožňuje akustická holografie v blízkém poli detailní popis pole nejen na měřené ploše, ale také kdekoli v okolním volném prostoru. Navíc, díky schopnosti zachycení evanescentních vln (přítomných pouze v blízkém poli zdroje) a jejich rekonstrukci poskytuje oproti klasickým metodám výrazně vyšší prostorové rozlišení. V práci je popsán matematický aparát popisující vyzařování zvuku do okolního prostoru - Helmholzova integrální rovnice a první a druhá Rayleighova integrální rovnice, přičemž úroveň odvození těchto vztahů je zvolena tak, aby byla patrná oblast platnosti popisované metody. Akustická holografie v blízkém poli je inverzní úloha plynoucí z inverze zmiňovaných vztahů popisujících vyzařovaní zvuku. Jelikož korektní řešení této úlohy vyžaduje regularizaci přenosových funckcí (matic) je základní popis regularizačních technik uveden v této práci. Dále je popsána metoda akustická holografie v blízkém poli využívající prostorovou Fourierovu transformaci pro planární a sférické souřadnice a dvě metody založené na minimalizaci odchylky aproximace naměřených akustických veličin modelovými bázovými funkcemi metodou nejmenších čtverců. V praktické části jsou uvedeny výsledky jak modelových simulací, tak experimentálních měření.

Klíčová slova: akustika, akustická holografie v blízkém poli, zvukové pole

Překlad názvu: Lokalizace zdrojů zvuku v uzavřených prostorech

Contents

Figures

Tables

Chapter 1

Introduction

In this chapter, the contemporary state of the sound field mapping, the aims of the thesis and chapter survey are stated.

1.1 Contemporary state of sound field mapping

A wide range of diverse techniques for spatial measuring (mapping) of the sound field has been developed during the past several decades. Commonly based on the spatial sampling of the sound field in several positions, these techniques provide information usable for localization and quantification of the sound sources, as well as, more recently, for evaluating new room acoustic parameters. Knowledge of the source's position and strength is essential in many applications; moreover, the possibility of distinguishing individual radiating parts of the source could be used to reduce overall radiated noise or reveal defective components. The usability of such techniques in various practical applications, in which a complex physical model including the effects such as sound reflections, diffraction and/or scattering has to be considered, are the subjects of ongoing research and investigation.

In general, two main approaches could be distinguished according to the distance between the source(s) and the measurement array. These are the Beamforming technique, first introduced by Billingsey et al. [1], and the technique of Nearfield Acoustical Holography (NAH) [2, 3, 4, 5]. The former

usually takes place far from the source(s) providing directional information of the surrounding field, whereas the latter is based on the measurement in the proximity of the source and the following reconstruction of the acoustic quantities on its surface. The main advantage of beamforming is the robustness of the method, while the drawbacks are its resolution limitations at low frequencies, its low dynamic range/resolution, and its lack of accuracy for quantifying acoustic source strengths. On the other hand, because of the reconstruction of the evanescent part of the sound field (non-radiating part measured close to the source surface), NAH excels in spatial resolution, yet such an exponential amplification is very sensitive to the presence of noise and the process of reconstruction has to be regularized.

Although various configurations of the measurement array (planar, cylindrical, spherical ...) are usable for both techniques, the subsequent signal processing usually differs. The original implementation of NAH is based on the Discrete Fourier Transform and in spite of its advantages (ease of implementation and low computational requirements) it is impractical in most cases due to the limitations described in [6]. Other methods based on the elementary wave models (planar [7] or spherical waves [8, 9]) have been developed to overcome these limitations. These wave models are used to fit the measured field by means of the least squares, and then project it back towards to the source. The main disadvantage of such wave model fitting methods is that they need not converge to the correct solution even for the noiseless data. Several patch algorithms have been also proposed to overcome the aperture size limitation of the original implementation [10, 11]. Some experiments dealing with the laser scanning vibrometer measurement of the normal component of the velocity of the very thin membrane placed near the source surface have been presented [12]. This approach offers very high spatial resolution, but due to the scanning nature it is limited to time-stationary sources. The most accurate implementation of NAH is based on the Boundary Element Method (BEM), yet unfortunately the computational requirements make it unsuitable in some situations [13]. The back-propagation of the sound field (towards to the source or identically back in the time) represents an ill-posed inverse acoustic problem according to the Hadamard conditions of existence, uniqueness and continuous dependence of the results on the measured data. As was mentioned above, this ill-posed circumstance is caused by the exponential amplification of the evanescent part of the sound field. In the practical implementation, this leads to the appearance of ill-conditioned transfer matrices that have to be regularized. Several regularization techniques exist, particularly Tikhonov regularization [14], and plenty of methods for the regularization parameter estimation such as the Morozov Discrepancy Principle, Generalized Cross Validation, L-curve criterion or Normalized Cumulative Periodogram [15]. Performing measurements in the near field of the source and capturing a sufficient amount of evanescent components (which decay exponentially and could be successfully captured only up to

the certain distance from the source surface that is inversely proportional to the frequency of interest) is essential for the high spatial resolution of NAH.

It is obvious from the above-mentioned brief description of the evolution of these various implementations that the theoretical background of sound field reconstruction, as well as the level of development of the implementations, has reached a high degree, since one of the first articles has been published. Nevertheless, the NAH is not yet commonly used in practice, mainly due to its relatively high cost and its low robustness in complex practical situations (small enclosed spaces, e.g. car cabin), where the strong reverberant field can occur. The basic planar arrays with pressure microphones (omnidirectional) are not able to work properly in such a field. Several approaches have been suggested to overcome this issue for the planar arrays. First is the use of the Microflown sensors [16, 17] capable of distinguishing the direction of the wave propagation. Second is the use of the multi-layer(s) microphone array [18] consisting of pressure microphones. The main advantage of these approaches is that the planar array is the most appropriate for many real sources (which are also planar or nearly planar). The drawbacks are the increased number of sensors and the directionality of the array (which still omits some directions). Another possible way to correctly localize sources in a reverberant field could take into account several different measurement positions (e.g. by moving an array to a different position). However, the stationary sound field has to be evaluated.

Recent studies dealing with localization and reconstruction in the reverberant field employ the spherical microphone array. The main advantage of the spherical configuration is its three-dimensional symmetry, and thus such an array takes into account the sound coming from any direction (which could also be steered to any direction using the appropriate signal treatment if necessary). The spherical array could be advantageously used in sound-field recording [19], beamforming or sound-field analysis including reconstruction of the sound field around the sphere or room acoustic parameters measurement [20, 21, 22, 23, 24]. The design of the spherical microphone array is closely related to the subsequent mathematical apparatus used during the signal processing and the assumed use of the array. Currently, two opposite constructions of the sphere are employed; the open sphere (acoustically transparent, no scattering effect is considered) and the rigid sphere. The former sphere could be used for both inverse and forward problems in both interior and exterior domains, assuming that all the sources are located outside and inside of the sphere (or the spheres of bigger and smaller radius, respectively). The open sphere could be also used advantageously in room acoustics measurements, in which the measurement of lower frequencies is of interest (because such frequencies are more accurately measured by the array

of bigger radius, thus the rigid sphere becomes impractical to realize). It is also worth mentioning that an open configuration could be, in comparison to the rigid sphere, relatively easily realized by an automatic scanning system (in the stationary sound field, very much so). The major drawback of an open configuration is that it suffers from ill-conditioning around the zeros of the spherical Bessel functions making the reconstruction impossible at certain combinations of wavenumber and radius (composing an argument of these functions). Some suggestions have been proposed to overcome this issue while maintaining an open sphere configuration, particularly the use of the complementary measurement of the particle velocity, of cardioid instead of omnidirectional microphones, of the dual-sphere configuration or the application of non-equidistant sampling in the frequency domain [25]; these other ways are still topics of current research. Another approach is to use a rigid sphere which improves the numerical conditioning as a consequence of counting with the scattering effect [23]. The total field around the rigid sphere is composed of the incident field and the field scattered by its surface. Therefore, before the employing of such techniques as beamforming or NAH, the separation of the incident field alone has to be carried out. Separation could be based on the different wave assumptions (e.g. plane or spherical) depending on the mutual positions of the source(s) and the array and geometry of the source. The theoretical framework and comparison of the plane and spherical waves scattered on the rigid spherical surface is presented in [26]. The main difficulty in connection with the field separation, which has become more critical since the spherical array has found utilization in NAH (the sources are close to the array), is the multiple reflection from the array and source surface(s) and the influencing of its radiation impedance by the presence of the array. This task is the subject of further study and is one of the main parts dealt with in this project. In principle the rigid sphere, could be used even in both the interior and exterior domains, nonetheless, it is obvious that its application is aimed at both inverse and forward problems in the interior domain.

Barring the above-mentioned properties of the rigid and open sphere configurations, another great challenge involves the distribution of a certain number of sensors around the spherical surface (sampling on the sphere). This task could be found in many fields of science such as geophysics, quantum chemistry or astrophysics, to mention just a few. It is common requirement that the array should be rotationally symmetrical. As mentioned in the previous paragraph, the design is usually closely connected to the subsequent analysis. Used not only in acoustics, this analysis is based on the decomposition of the measured data into the spherical harmonic functions (spherical harmonics) using the spherical Fourier transform [6]. The spherical harmonics are composed of the standing spherical waves in the elevation direction (described by the associated Legendre functions of certain degrees and orders) and by the traveling spherical waves in the azimuth direction (described by the complex exponential functions depending also on the degree

of spherical harmonics). Broadly speaking, the higher the order is of spherical harmonics, the better the spatial resolution results. It follows that the next requirement after the sensors' placement is that it should ensure the exact representation of a band-limited signal. In other words, it should ensure that the discrete representation of the integral Fourier transform (around the sphere surface) by the sum over a finite number of positions provides an exact computation of the Fourier coefficients. Conversely, it should also ensure that the inverse Fourier transform represented by the sum of the spherical harmonics functions multiplied by these coefficients will equal to the original signal even if the summation is performed up to the finite number (maximum order). Probably the most common methods for distributing points on the sphere are equiangle sampling, nearly uniform sampling and Gaussian sampling (Gaussian quadrature) [23]. More information concerning this topic could be found in [27] and [28], whereas some novel techniques are discussed e.g. in [29] or [30]. Except for the positions, the number of sensors determines the highest order of the spherical harmonics that can be precisely represented (in which case we talk about the spherical array of certain order). However, the above-mentioned assumption of a band-limited signal is not valid e.g. in such a simple case as the plane wave (which is decomposed into the infinite number of the spherical waves) [31]. This circumstance leads to the constant development of methods for reducing the influence of aliasing such as presented in [32], as well as different approaches of the signal representation (e.g. wavelets) discussed together with the appropriate sampling on the sphere.

The localization of sound sources in the complex reverberant fields is the subject of current research, and also the principal purpose of this project. As mentioned, the spherical array has the ability to deal with the sound field coming from any direction and thus it is the most convenient array for operating under such conditions. Sound field analysis by plane wave decomposition and sound source localization using the beamforming technique is presented in [22]. A comprehensive theoretical description of the sound field reconstruction using the spherical array measurement can be found mainly in [6]. Recently, the reconstruction of an acoustic intensity vector in the volume (not only in one point, as is usual for the classical two-microphone arrangement or three-dimensional probe) has been presented for both open [33] and rigid spheres [34]. The reconstruction of incident acoustic pressure alone has been investigated in [35] considering the plane waves scattered on the rigid sphere. The spherical array configuration has been recently used as well for the new room acoustic parameters measurement [[24], [36]]. In comparison to the traditional room acoustic parameters, these new parameters (e.g. directional diffusion) include directional information about the reverberant field which could be used for the evaluation of reflection and initializing of specific parameters before processing.

1.2 Aims of the thesis

Nearfield acoustical holography is a very promising method providing an exceptional information for sound source(s) localization, radiated sound power estimation, machinery defective part(s) non-contact localization and evaluation, etc. Despite its powerful attributes, it is not commonly used in practice nowadays mainly due to its relatively high measurement and computational requirements and related cost requirements. Several techniques to overcome various method difficulties have been developed and are still the subjects of present and future research. The aims of this thesis are to examine the possibilities overcoming mainly the difficulties related to a large number of measurement points needed, the computational requirements of previously proposed methods and problems arising form the finite aperture (using the spherical microphone array). An evaluation of this examination could serve as a base for further research possibilities.

This theses and experiments performed has been supported by the CTU research project SGS13/193/OHK3/3T/13 Monitoring and modeling methods in acoustics and by the CTU student project No. SGS16/221/OHK3/3T/13 “Measurement, modeling and evaluation methods in acoustics”.

1.3 Chapter survey

The thesis is divided into two parts - theoretical and practical. In the theoretical part the Helmholtz integral equation and the first and second Rayleigh integral equation describing the sound radiation are first derived. Then the regularization techniques as well as the regularization parameter choice methods are briefly described in chapter 3. In chapter 4, the nearfield acoustical holography is described for the Fourier-based approach for planar and spherical coordinates and for the approach based on the least squares minimization (SONAH and HELS). In the practical part in chapter 5, the results based on authors publications are presented. Firstly the sound field reconstruction using the combined elementary wave model is presented, followed by the reconstruction based on the laser scanning vibrometer measurement on an acoustically induced thin membrane. Then the sound field reconstruction employing the rigid sphere is presented. At the end, a source distance estimation based on the spherical harmonics is stated. Chapter 6 summarize the conclusions. Graphic presentations of the results are stated in the appendices.

Part I

Theoretical Part

The theory of sound is very broad, encompassing a great variety of mechanism of its origin as well as the radiation under a diverse conditions. In a very general description, any object could radiate sound into the surrounding media depending on both the disturbance and media parameters. The radiation of sound belongs to the forward acoustics problems and it is well described by the Helmholtz integral equation (HIE) and its modifications using Rayleigh integral equations. The forward acoustics problems generally describes the problems in which the cause (acoustic source vibration) is known and the effect (radiation; the sound field at any point in the space) is sought. These problems are usually mathematically well-posed, meaning that the underlying mathematical model describing a physical problem satisfy certain conditions ensuring its solvability. These conditions were formulated by Jacques Hadamard as follows:

1. a solution must exist,
2. a solution must be unique,
3. a solution must continuously depend on the data.

Such a problem is then mathematically termed as well-posed. When any of these conditions is violated, the problem is ill-posed. The inverse (acoustic) problems needs to be solved with caution and some additional controls have to be taken into account. These additional controls are in relation to inverse problems commonly mathematically termed as regularization. The forward acoustics problems are typically well-posed because the transfer function relating two points in the space attenuates according to its distance the radiated sound field.

It is the fundamental task of majority of acoustics measurement techniques to describe the sound field radiated by a source under interest and possibly reveal this source and its origin (cause). Basic and well-established techniques provide a map of most of the sound power radiation areas or a map of sound energy flow based on the measurement of active acoustic intensity (directly or individually using measurement of acoustic pressure and acoustic particle velocity). These techniques are often sufficient for an evaluation of the radiated sound field, however, they usually do not provide enough information about the sound source and its origin. Therefore, more sophisticated techniques have been developed to be able to provide these information. This technique, the so-called Nearfiled Acoustical Holography (NAH), is the subject of this thesis.

The NAH belongs among the **inverse acoustics problems** and solves the unknown cause (acoustic source vibration) based on the known effect

(measured radiated sound field). Many inverse acoustics problems (many inverse problems in general - not only in acoustics) are ill-posed mainly because of their violation. While a violation of any of the first two conditions is usually caused by an improper problem statement or use of the wrong mathematical model, a violation of the third condition is most often caused by the application of the inverse transfer function to the data contaminated by a noise. In the NAH specifically, the ill-posedness is caused by the presence of the so-called evanescent waves. These types of acoustic waves are exponentially attenuated depending on the distance from the sound source and oppositely amplified by an inverse transfer function while performing the NAH procedure.

First, the sound radiation is briefly surveyed followed by the general description of the inverse problems and its regularization. Then, the description of the NAH is stated. The very general equations of linear acoustics including the Euler equation, equation of continuity, Poisson equation as well as the wave equation are not explicitly stated in this thesis, since it is assumed they are familiar to the reader.

Chapter 2

Sound Radiation

In this section the fundamental equations constituting the sound radiation are described - the Helmholtz integral equation and the Rayleigh integral equation. The level of description should provide a trackable derivation of the equations stated and make the concept of the NAH obvious.

2.1 Green's Theorem

Green's theorem (Green's second identity) describes the relation of the physical field on the (integrable) surface and the field in a volume bounded by this surface. Physically, this theorem states that the energy arising in this volume must equal to the energy flow through the surface enclosing this volume. To derive Green's theorem we start with Gauss's theorem

$$\oiint_S \boldsymbol{E} \cdot \boldsymbol{n} \, \mathrm{d}S = \iiint_V \operatorname{div} \boldsymbol{E} \, \mathrm{d}V, \tag{2.1}$$

where $\boldsymbol{E}$ is a vector quantity, S and V are the integration surface and volume, respectively, and div stands for the divergence. Consider finite and continuous along with their first and second derivatives scalar functions ψ and ϕ satisfying the homogenous Helmholtz equation

$$\nabla^2 \psi + k^2 \psi = 0, \qquad \nabla^2 \phi + k^2 \phi = 0. \tag{2.2}$$

Based on the functions ψ and ϕ define vector functions

$$\boldsymbol{E} = \psi \operatorname{grad} \phi,$$

$$\boldsymbol{F} = \phi \text{ grad}\, \psi.$$

Inserting functions $\boldsymbol{E}$ and $\boldsymbol{F}$ into Gauss's theorem (2.1) results in

$$\oiint_S \psi \text{ grad}\, \phi \, \boldsymbol{n} \, \mathrm{d}S = \iiint_V \text{div}\, (\psi \text{ grad}\, \phi)\, \mathrm{d}V,$$

$$\oiint_S \phi \text{ grad}\, \psi \, \boldsymbol{n} \, \mathrm{d}S = \iiint_V \text{div}\, (\phi \text{ grad}\, \psi)\, \mathrm{d}V,$$

where $\mathrm{d}S$ is the surface integral element and $\boldsymbol{n}$ is the unit normal vector. Rewriting using well-known identities[1] results in

$$\oiint_S \phi \frac{\partial \psi}{\partial n} \, \mathrm{d}S = \iiint_V (\text{grad}\, \phi \text{ . } \text{grad}\, \psi + \phi \, \nabla^2 \psi)\, \mathrm{d}V,$$

$$\oiint_S \psi \frac{\partial \phi}{\partial n} \, \mathrm{d}S = \iiint_V (\text{grad}\, \psi \text{ . } \text{grad}\, \phi + \psi \, \nabla^2 \phi)\, \mathrm{d}V.$$

Substracting both equations lead to **Green's theorem**

$$\oiint_S (\phi \frac{\partial \psi}{\partial n} - \psi \frac{\partial \phi}{\partial n}) \, \mathrm{d}S \; = \iiint_V (\phi \nabla^2 \psi - \psi \nabla^2 \phi)\, \mathrm{d}V, \tag{2.3}$$

where $\frac{\partial}{\partial n}$ is the derivative with respect to the surface outward normal vector. Based on the assumption that both functions ψ and ϕ satisfy the homogenous Helmholtz equation (no energy arising nor energy loss), the right hand side equals to zero and the equation (2.3) reduces to form

$$\oiint_S (\phi \frac{\partial \psi}{\partial n} - \psi \frac{\partial \phi}{\partial n}) \, \mathrm{d}S = 0. \tag{2.4}$$

Using the Eq.(2.4) we derive the Helmholtz integral equation.

2.2 Helmholtz Integral Equation

Deriving the Helmholtz integral equation (HIE) slightly differs for the **interior** or **exterior domain**. The solution for the interior domain provides

[1]
$$\text{grad}\, \psi \boldsymbol{n} \, \mathrm{d}S = \frac{\partial \psi}{\partial n} \, \mathrm{d}S,$$
$$\text{grad}\, \phi \boldsymbol{n} \, \mathrm{d}S = \frac{\partial \phi}{\partial n} \, \mathrm{d}S,$$
$$\text{div}\, (\phi \text{ grad}\, \psi) = \text{grad}\, \phi \text{ . } \text{grad}\, \psi + \phi \, \nabla^2 \psi,$$
$$\text{div}\, (\psi \text{ grad}\, \phi) = \text{grad}\, \psi \text{ . } \text{grad}\, \phi + \psi \, \nabla^2 \phi$$

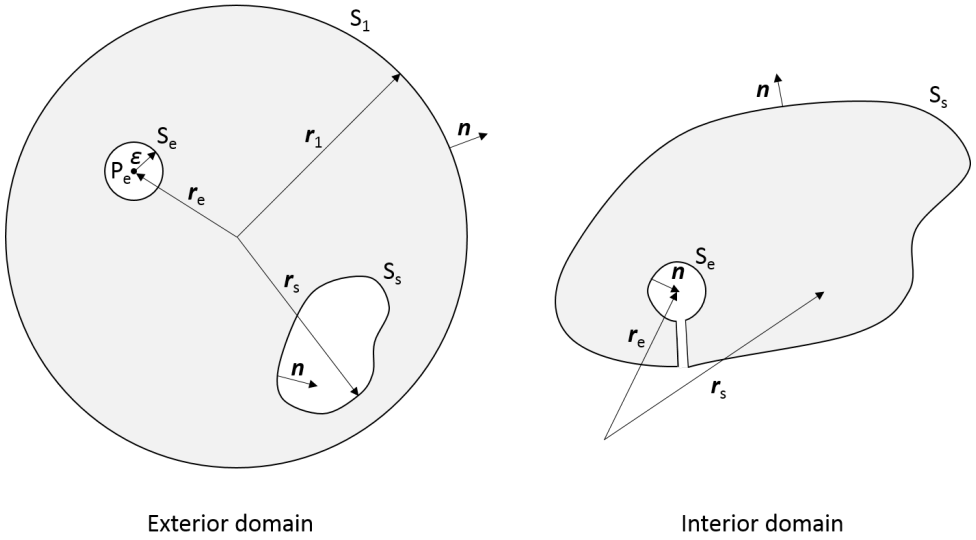

Figure 2.1: Exterior and interior domain

an acoustic field evaluation in a volume enclosed by a surface on which the acoustic quantities are known (e.g. observed) while all the sound source are located outside this volume. On the other hand, the solution for the exterior domain provides an acoustic field evaluation everywhere in a source-free region based on the known acoustic quantities on the surface surrounding the sound source(s).

2.2.1 Exterior domain

Assume a sphere S_1 of radius $|\boldsymbol{r}_1|$ which tends towards infinity, a sphere S_e of radius $|\boldsymbol{r}_e|$ surrounding the field evaluation point P_e and a volume containing all sound sources enclosed by a surface S_s on which the acoustic quantities are known (observed). The situation is depicted in Fig. 2.1. For deriving the HIE we start with Eq.(2.4), in which the function ϕ describes the observed acoustic field and thus satisfies the homogenous Helmholtz equation, (Eq.2.2). Consider a function ψ relating the acoustic field quantity at the observed and evaluation point. Such a function satisfies the non-homogenous Helmholtz equation

$$\nabla^2\psi + k^2\psi = -\delta(\boldsymbol{r}_s - \boldsymbol{r}_e), \tag{2.5}$$

where δ is the Dirac delta function representing the point source. The solution of Eq.(2.5) is the **free-space Green's function**

$$\psi = G(\boldsymbol{r}_s|\boldsymbol{r}_e) = \frac{e^{-\mathrm{j}k|\boldsymbol{r}_s - \boldsymbol{r}_e|}}{4\pi|\boldsymbol{r}_s - \boldsymbol{r}_e|}. \tag{2.6}$$

Despite its dependance on the wavenumber k, the form $G(\boldsymbol{r}_\mathrm{s}|\boldsymbol{r}_\mathrm{e})$ expressing its spatial dependance will be used for notation simplicity in the latter. Due to the singularity of the free-space Green's function for $|\boldsymbol{r}_\mathrm{s} - \boldsymbol{r}_\mathrm{e}| \to 0$, when

$$\lim_{|\boldsymbol{r}_\mathrm{s}-\boldsymbol{r}_\mathrm{e}|\to 0} \frac{e^{-jk|\boldsymbol{r}_\mathrm{s}-\boldsymbol{r}_\mathrm{e}|}}{|\boldsymbol{r}_\mathrm{s} - \boldsymbol{r}_\mathrm{e}|} = \infty,$$

it is necessary to modify the integrafion surface in Eq.(2.4) to exclude the singular point. The modification leads to the integration over three surfaces, which can be symbolically stated as

$$\oiint_{S_1} \left[\phi \frac{\partial}{\partial n} G(\boldsymbol{r}_\mathrm{s}|\boldsymbol{r}_\mathrm{e}) - G(\boldsymbol{r}_\mathrm{s}|\boldsymbol{r}_\mathrm{e}) \frac{\partial \phi}{\partial n}\right] \mathrm{d}S_1 + \oiint_{S_\mathrm{e}} [\cdots] \, \mathrm{d}S_\mathrm{e} + \oiint_{S_\mathrm{s}} [\cdots] \, \mathrm{d}S_\mathrm{s} \; = 0. \tag{2.7}$$

Restating the integration over the surface S_1 leads to

$$\oiint_{S_1} \left[\phi \frac{\partial}{\partial n} G(\boldsymbol{r}_\mathrm{s}|\boldsymbol{r}_\mathrm{e}) - G(\boldsymbol{r}_\mathrm{s}|\boldsymbol{r}_\mathrm{e}) \frac{\partial \phi}{\partial n}\right] \mathrm{d}S_1 = - \lim_{|\boldsymbol{r}_\mathrm{s}-\boldsymbol{r}_\mathrm{e}|\to\infty} e^{\mathrm{j}k\,|\boldsymbol{r}_\mathrm{s}-\boldsymbol{r}_\mathrm{e}|} \boldsymbol{r}_\mathrm{s} \left[\frac{\partial \phi}{\partial \boldsymbol{r}_\mathrm{s}} - \mathrm{j}k\phi\right],$$

in which the following part of the right hand side

$$\lim_{|\boldsymbol{r}_\mathrm{s}-\boldsymbol{r}_\mathrm{e}|\to\infty} \boldsymbol{r}_\mathrm{s} \left[\frac{\partial \phi}{\partial \boldsymbol{r}_\mathrm{s}} - \mathrm{j}k\phi\right] = 0 \tag{2.8}$$

represents the boundary condition known as the Sommerfeld radiation condition at infinity. Restating the integration over the surface S_e for the limiting case of sphere radius $\epsilon \to 0$ leads to

$$\lim_{\epsilon\to 0} \oiint_{S_\mathrm{e}} \left[\phi \frac{\partial}{\partial n} G(\boldsymbol{r}_\mathrm{s}|\boldsymbol{r}_\mathrm{e}) - G(\boldsymbol{r}_\mathrm{s}|\boldsymbol{r}_\mathrm{e}) \frac{\partial \phi}{\partial n}\right] \mathrm{d}S_\mathrm{e} = \alpha\phi(\boldsymbol{r}_\mathrm{e}), \tag{2.9}$$

where

$$\alpha = \begin{cases} 1 & \text{for } \boldsymbol{r}_\mathrm{e} \text{ outside } S_\mathrm{s} \\ 1/2 & \text{for } \boldsymbol{r}_\mathrm{e} \text{ on } S_\mathrm{s} \\ 0 & \text{for } \boldsymbol{r}_\mathrm{e} \text{ inside } S_\mathrm{s} \end{cases}.$$

Inserting these particular results into the Eq.(2.7) lead to the **Helmholtz integral equation**.

$$\oiint_{S_\mathrm{s}} \left[G(\boldsymbol{r}_\mathrm{s}|\boldsymbol{r}_\mathrm{e}) \frac{\partial \phi(\boldsymbol{r}_\mathrm{s})}{\partial n} - \phi(\boldsymbol{r}_\mathrm{s}) \frac{\partial}{\partial n} G(\boldsymbol{r}_\mathrm{s}|\boldsymbol{r}_\mathrm{e})\right] \mathrm{d}S_\mathrm{s} = \alpha\phi(\boldsymbol{r}_\mathrm{e}). \tag{2.10}$$

2.2.2 Interior domain

The derivation of HIE for the interior domain is analogous to the exterior domain assuming again a sphere S_e surrounding the field evaluation point

and a surface S_s on which the acoustic quantities are known (observed). For the interior domain, however, all the sources are located outside the volume surrounded by this surface in which the acoustic quantities could be evaluated. The situation is depicted on the right side in Fig. 2.1. The solution differs from Eq. (2.10) only by its validity depending on the location of the evaluation point, thus

$$\alpha = \begin{cases} 1 & \text{for } \boldsymbol{r}_\mathrm{e} \text{ inside } S_\mathrm{s} \\ 1/2 & \text{for } \boldsymbol{r}_\mathrm{e} \text{ on } S_\mathrm{s} \\ 0 & \text{for } \boldsymbol{r}_\mathrm{e} \text{ outside } S_\mathrm{s} \end{cases} .$$

Thorough derivation of the HIE for interior domain could be found in [6].

2.3 Rayleigh Integral Equation

It is evident that solving the Helmholtz integral equation both function ϕ and its normal derivative are necessary. In other words, the knowledge of both acoustic pressure and particle velocity on the integration surface are needed to evaluate acoustic pressure at the evaluation point. Examining the HIE it is potential to reduce this "over-specification" by restricting the Green's function using the appropriate boundary condition. Two possibilities are used, the first, known as Dirichlet's boundary condition, prescribes the boundary condition $G \equiv G_\mathrm{D} = 0$ yielding to **the first Rayleigh integral formula**

$$\phi(\boldsymbol{r}_\mathrm{e}) = \oiint_{S_\mathrm{s}} \phi(\boldsymbol{r}_\mathrm{s}) \frac{\partial}{\partial n} G_\mathrm{D}(\boldsymbol{r}_\mathrm{s}|\boldsymbol{r}_\mathrm{e}) \,\mathrm{d}S_\mathrm{s}, \tag{2.11}$$

and the second, known as Neumann's boundary condition, prescribes the boundary condition $\partial G/\partial n \equiv \partial G_\mathrm{D}/\partial n = 0$ yielding to **the second Rayleigh integral formula**

$$\phi(\boldsymbol{r}_\mathrm{e}) = -\oiint_{S_\mathrm{s}} G_\mathrm{N}(\boldsymbol{r}_\mathrm{s}|\boldsymbol{r}_\mathrm{e}) \frac{\partial \phi(\boldsymbol{r}_\mathrm{s})}{\partial n} \,\mathrm{d}S_\mathrm{s}. \tag{2.12}$$

The Rayleigh integrals describes the sound field radiated by the sound source(s) and their validity follow from solving the HIE for the exterior domain (note, that parameter α has been omitted since its relevance is obvious). Substituting the acoustic pressure $p(\boldsymbol{r})$ instead of the function ψ in Eq.(2.11) and (2.12) the Rayleigh integrals could be expressed as

$$p(\boldsymbol{r}_\mathrm{e}) = -\oiint_{S_\mathrm{s}} p(\boldsymbol{r}_\mathrm{s}) \frac{\partial}{\partial n} G_\mathrm{D}(\boldsymbol{r}_\mathrm{s}|\boldsymbol{r}_\mathrm{e}) \,\mathrm{d}S_\mathrm{s} \tag{2.13}$$

and

$$p(\boldsymbol{r}_\mathrm{e}) = \mathrm{j}\rho c k \oiint_{S_\mathrm{s}} v_n(\boldsymbol{r}_\mathrm{s}) G_\mathrm{N}(\boldsymbol{r}_\mathrm{s}|\boldsymbol{r}_\mathrm{e}) \,\mathrm{d}S_\mathrm{s}, \tag{2.14}$$

respectively. Note that the well-known Euler equation has been used to derive the Eq.(2.14) in the expressed form. The Eq.(2.13) and (2.14) both enable to evaluate acoustic pressure at the evaluation point $p(\boldsymbol{r}_\mathrm{e})$ based on the knowledge of acoustic pressure or particle velocity, respectively, on the surface S_s. The Rayleigh integral equations as well as the HIE represent a forward acoustics problem. To solve the inverse acoustics problem these equations need to be inverted. The inversion of these equations (especially the Rayleigh integral equations) is the main subject of the nearfield acoustical holography [6].

Chapter 3

Inverse Problems and Regularization

In this section, an overview of the inverse problems and methods of their solution is stated. The description follows the general definitions of well-posed/ill-posed problems as well as Hadamard's conditions stated in the introduction of this part of the thesis.

It is very common when dealing with a physical problems that the relation between the cause and the effect is mathematically described using an integral equation. One class of such physical problems share the underlying mathematical model described using **the Fredholm integral equation of the first kind**

$$g(e) = \int_a^b K(s,e) f(s)\,\mathrm{d}s, \tag{3.1}$$

where the kernel K relates the function f and g and describes the underlying physical model (e.g. sound wave propagation) valid in some domain specified using the integration limits (a, b). In case of a known function f (cause), the evaluation of the integral yields to the function g (effect) and represents the forward problem. On the other hand, finding the cause function f based on knowledge of the effect function g represents the inverse problem and requires the inversion of the Eq.(3.1). Note that in a special case when the kernel K is a function of the difference between s and e, the Eq.(3.1) represents the convolution (deconvolution for the inverse problem).

If the inversion of kernel function K satisfy all of Hadamard's conditions, the problem is well-posed and the cause function f can be evaluated. Otherwise, the problem is ill-posed and some additional requirements (regularization) need to be incorporated in order to attain meaningful solution of the function

f. As has been mentioned, a violation of any of the first two of Hadamard's conditions is usually caused by an improper or wrong problem definition (inaccurate or wrong physical model, not sufficient data acquisition etc.) and could be usually overcome as described later. The violation of the third condition is very frequent for many inverse problems (especially those represented by deconvolution) and its substance lies in amplifying high frequency components of the acquired data (the function g) by the inverse of the kernel K. These high frequency components in the acquired data are the smooth version of components in the source data (the function f) according to the Riemann-Lebesque lemma [14].

To solve the inverse problem described by Eq.(3.1) numerically, it is necessary to perform the discretization of the integral equation. Although the integral discretization methods are very important for the current topic and could provide unique properties for data acquisition procedure (especially in more complex geometries), only the references are stated in this thesis due to the extensiveness of this subject. The description of the quadrature and expansion methods could be found in [14] together with the discussion of which method to choose. The references regarding individual coordinate systems are stated in the corresponding sections of the thesis. Rewriting the Eq.(3.1) in a discrete form yields

$$\mathbf{g} = \mathbf{K}\mathbf{f}, \tag{3.2}$$

where vector $\mathbf{g} \in \mathbb{C}^m$ (resp. $\mathbf{f} \in \mathbb{C}^n$) contains samples of the function $g(e)$ (resp. $f(s)$) at corresponding discrete points of domain e (resp. s) and the matrix $\mathbf{K} \in \mathbb{C}^{m \times n}$ relates these functions depending on the sampling points and the underlying physical model. In the latter we will assume $m \geq n$. It can be easily showed from the theory of the system of linear equations (such as Eq.(3.2)) that assuming $m = n$ the solution of $\mathbf{f} = \mathbf{K}^{-1}\mathbf{g}$ is very sensitive to the noise in the vector $\mathbf{g}$ and, moreover, that the solution possibly do not even exists. Instead of solving the system of linear equation, the least square problem (valid for $m \geq n$)

$$\min_{f} ||\mathbf{K}\mathbf{f} - \mathbf{g}||_2 \tag{3.3}$$

is considered to yield the solution. Even though the solution exists, the additional restrictions on the result (such as $\min ||\mathbf{f}||_2$) need to be incorporated to ensure its uniqueness.

3.1 Regularization methods

A very powerful tool to regularize the (discrete) inverse problems is the singular value decomposition (SVD), which for a real or complex matrix $\mathbf{A}$

takes the form

$$\mathbf{A} = \mathbf{U}\mathbf{\Sigma}\mathbf{V}^{\mathrm{H}} = \sum_{i=1}^{n} \mathbf{u}_i \sigma_i \mathbf{v}_i^{\mathrm{H}}, \tag{3.4}$$

where matrix $\mathbf{U}$ consist of the left singular vectors, matrix $\mathbf{V}$ consists of right singular vectors and matrix $\mathbf{\Sigma}$ is the diagonal matrix consisting of the singular values. The letter H states for the matrix Hermitian transposition. It is commonly assumed that the singular values are ordered such that $\sigma_1 > \sigma_2 > \ldots > \sigma_n$. The properties of SVD are well-known and could be found in many fundamental linear algebra publications such as [37] and [38]. Having computed the SVD, it is straightforward to compute the inversion of matrix $\mathbf{A}$ as

$$\mathbf{A}^{-1} = \mathbf{V}\mathbf{\Sigma}^{-1}\mathbf{U}^{\mathrm{H}}. \tag{3.5}$$

In connection with the ill-posed inverse problems, it is useful to quantify its ill-posedness using the singular values as

$$\mathrm{cond}(\mathbf{A}) = \frac{\sigma_1}{\sigma_n}, \tag{3.6}$$

where $\mathrm{cond}(\mathbf{A})$ is the matrix condition number. According to the definition and the fact that $\sigma_1 \geq \sigma_n$, the condition number must satisfy $\mathrm{cond}(\mathbf{A}) \geq 1$. Closer the condition number to one, the better the inverse problem is posed. The decreasing character of the singular values is related to mentioned Riemann-Lebesque lemma. The rate of change of the singular vectors (the number of zero value passing) increases with increasing order (i in Eq.(3.4)) of the singular values accounting for the higher frequency component of the data. Note that these components do not directly represent any physical phenomenon contained in the data since their orthonormal property arising from the SVD. It is evident that these high frequency components carry detailed information necessary to solve the inverse problem with sufficient resolution. It is also evident that the amount of noise in these components is determining its usability. Controlling the impact of these components on the solution is the main task of the regularization techniques. Although the SVD could be directly used to regularize the inverse problems (such as the truncated SVD described in the next section), it should be noted that there are other methods that do not use it directly - mainly due to its possible high computational demands especially for large-size matrices. Nonetheless, in any case it is a very powerful tool not only for the data inspection but also for evaluation as well as the understanding of the method's performance.

Using the Eq.(3.5), the solution of the inverse problem Eq.(3.2) can be formulated as

$$\mathbf{f} = \mathbf{K}^{-1}\mathbf{K} = \sum_{i=1}^{n} \frac{\mathbf{u}_i^{\mathrm{H}}\mathbf{K}}{\sigma_i}\mathbf{v}_i. \tag{3.7}$$

3.1.1 Truncated SVD

The truncated SVD is a method directly influencing the singular values by means of finding the value $k \leq n$ determining the maximal order of the singular values such that

$$\mathbf{f}_k = \sum_{i=1}^{k} \frac{\mathbf{u}_i^{\mathrm{H}}\mathbf{K}}{\sigma_i}\mathbf{v}_i. \tag{3.8}$$

The value k is usually estimated using the comparison of the singular values and noise variance. This method can be seen as a sharp filter taking the value 1 or 0 for individual singular values. The advantage is its implementation simplicity, however, due to its filtering sharpness, it does not usually provide an optimal solution.

3.1.2 Tikhonov regularization

One of the best-know regularization methods is the Tikhonov regularization.

$$\mathbf{f}_\alpha = \min_{\mathbf{f}} ||\mathbf{K}\mathbf{f} - \mathbf{K}||_2^2 + \alpha^2 ||\mathbf{L}\mathbf{f}||_2^2, \tag{3.9}$$

where α is the regularization parameter, $\mathbf{L}$ is the Tikhonov matrix (influencing the smoothness of a solution; often the identity matrix $\mathbf{I}$) and the symbol $||.||_2$ stands for the Euclidean norm. The first part represents the residual norm while the second part represents the side constraint that restricts the regularized solution to a required boundary – determined by the regularization parameter. The solution of Eq.(3.9) in a standard form ($\mathbf{L} = \mathbf{I}$) can be found as

$$\mathbf{f}_\alpha = (\mathbf{K}^{\mathrm{H}}\mathbf{K} + \alpha^2\mathbf{I})^{-1}\mathbf{K}^{H}\mathbf{K}, \tag{3.10}$$

where symbol H is the conjugate transpose of the matrix and one can recognize the Moore-Penrose pseudoinverse $\mathbf{K}^{+} = (\mathbf{K}^{\mathrm{H}}\mathbf{K})^{-1}\mathbf{K}^{\mathrm{H}}$. It can be easily shown that employing the SVD the solution of minimization problem (Eq.(3.9)) can be stated in a form similar to Eq.3.7 as

$$\mathbf{f}_\alpha = \sum_{i=1}^{n} \varphi_{i,\alpha} \frac{\mathbf{u}_i^{\mathrm{H}}\mathbf{K}}{\sigma_i}\mathbf{v}_i. \tag{3.11}$$

The filter factors $\varphi_{i,\alpha}$ are close to one for singular values $\sigma_i >> \alpha$ and asymptotically reach the value σ_i^2/α^2 for $\sigma_i << \alpha$. Therefore, the filter introduced by the Tikhonov regularization proportionally dampens the higher frequency components responsible for the ill-posedness of the inverse problem. A detailed explanation and examples of other methods can be found in [14]. The estimation of the regularization parameter α is essential for the required validity and credibility of the solution..

3.2 Regularization parameter estimation methods

It is evident from previous section that the regularization of the problem always depends on some decision level controlling the impact of higher frequency components to the solution – such as value k in truncated SVD regularization or the regularization parameter α in the Tikhonov regularization. Several regularization parameter estimation methods have been proposed and new are still being investigated. There is no universally superior method. For a given problem, the most adequate solution (the closest to the exact solution) will be in general achieved by exploiting as much as possible useful information contained in the measured data as well as by valid and exact description of the underlying physical model. Four regularization parameter estimation methods are stated in this section:

- Discrepancy principle
- L-curve criterion
- Generalized cross validation
- Normalized cumulative periodogram

An insightful description of these method could be found in [14].

3.2.1 Discrepancy principle

One of the basic methods is the Morozov Discrepancy Principle (MDP). This method requires a knowledge of the noise standard deviation δ (discrepancy), which is compared with the residual norm

$$||\mathbf{K}\mathbf{f}_{\text{reg}} - \mathbf{g}||_2 = \delta\sqrt{M}, \tag{3.12}$$

where M is the number of measurement points. Precisely filtering out the noise from the data, Eq.(3.12) leads to the definition of the variance of a random variable. The main advantage of this method is its simplicity (only the norm need to be evaluated). On the other hand, this method is very sensitive to the estimated value of the noise standard deviation and, therefore, robust method for its estimation need to be implemented.

3.2.2 L-curve criterion

This method is commonly called the L-curve criterion according to the shape of a curve resulting from a graphical representation of dependence of the regularized solution norm $||\mathbf{f}_{\text{reg}}||_2$ on the residual norm $||\mathbf{Kf} - \mathbf{g}||_2$ in Eq.(3.9) for variable regularization parameter. The objective is to estimate the regularization parameter corresponding to the "corner" of this curve. Although this method is very intuitive, finding the corner could be problematic for some kind of the inverse problems (not unique corner). Moreover, this method is not optimal in case of $\sigma \to 0$, because it does not converge to the exact solution [14].

3.2.3 Generalized cross validation

Another method that does not require the information about the noise is the Generalized Cross-Validation (GCV). Each time during an iterative process one value from the data is left out and substitute with a prediction based on the rest values. Then, the difference between the prediction and taken value is minimized for all possible combinations. This iterative process can be implemented advantageously by means of minimization of the functional

$$J(\alpha) = \frac{m||\mathbf{Kf}_{\text{reg}} - \mathbf{g}||_2^2}{\text{trace}(\mathbf{I} - \mathbf{KK}_{\text{reg}})^2}, \tag{3.13}$$

where m and trace(.) are the number of the elements on the main diagonal and their sum, respectively, and $\mathbf{K}_{\text{reg}}$ is a matrix that satisfy $\mathbf{f}_{\text{reg}} = \mathbf{K}_{\text{reg}}\mathbf{g}$. For $\alpha \to 0$ both numerator and denominator go to zero and the minimum of this ratio is sought for determining the regularization parameter. The advantage of this method is its needlessness to noise variance estimate and its formulation in a compact form of Eq. 3.13. Method has been firstly published in 1979 [39] in general concept. For acoustics source strength estimation the method has been described in [40] and [41], and especially for the NAH in [15].

3.2.4 Normalized cumulative periodogram

The idea of the Normalized Cumulative Periodogram (NCP) consists in comparing the spectrum of residual norm with the spectrum of the white

noise. Starting with the high regularization parameter α (influencing the regularized residual norm $||\mathbf{K}\mathbf{f}_{\text{reg}} - \mathbf{g}||_2$) and successive reducing its value, the normalized cumulative periodogram is computed as

$$C_i = \frac{\sum_2^{i+1} \mathbf{P}_i}{|\mathbf{P}| - P_0}, \qquad i = 1, 2, \ldots n-1 \tag{3.14}$$

where $\mathbf{P}$ is the power spectrum and P_0 is the mean value. Both the MDP and NCP are based on the idea to find the residual corresponding to the noise, however, the NCP is more sophisticated while considering statistical properties of the noise instead of only the norm.

Chapter 4

Nearfield Acoustical Holography

Sound source localization by Nearfield Acoustical Holography (NAH) is an approach that has been continuously developing since the 1960s. The original idea, for which the author received the Nobel Prize in Physics in 1971, comes from Hungarian scientist Dénes Gábor, who described the optical holography principle in 1948 during his work on electron microscopy. The principle of this technique in acoustics is computation of the sound field everywhere in the space based on the measurement of both an amplitude and a spatial phase of an acoustic quantity in several points in the space (measured data must be spatially correlated). However, the main application of this method is the localization of the sound source(s) in sense to compute (reconstruct) acoustic quantities on the vibrating surface(s) of the source based on the (non-contact) measurement of the sound field above the surface. This technique differs from other sound source localization techniques (i. e. beamforming) mainly in capturing the evanescent components in the near field of a sought source – thus, the nearfield attribute.

As mentioned in the previous chapter, such a task as trying to determine the cause of sound radiation represents an inverse acoustic problem. The corresponding forward problem is formulated by the Rayleigh's integral equations (2.12) and (2.11). Therefore, the inversion of Green's functions leads to the ill-conditioned matrices (in discrete form). NAH violates the third Hadamard's condition primarily by the presence of the noise in the evanescent components that are exponentially amplified during the reconstruction. Although this is one of the most serious problem, which must be regularized, the capturing of evanescent waves is essential for NAH, because they significantly increase the spatial resolution of reconstruction (their wavelengths are shorter than the corresponding acoustic wavelengths. Therefore, this technique is very sensitive to the noise in the measured quantities and the regularization

method must be applied and the regularization parameter must be finely determined.
The spatial resolution of the reconstruction depends principally on the spatial sampling of the sound field, which leads to the use of a huge number of sensors in array or an unacceptable long measuring time using a mechanical scanning system (for time-stationary sources). On the other hand, in case of a planar measurement surface, the size of measurement array (an aperture) determine the spatial low-frequency limit and in addition only the reconstruction of a part of the source surface directly below the array is correct. These limitations are caused by employing the spatial Fourier transform (Fourier-based NAH). Other methods trying to overcome these limitation have been developed – such as Statistically Optimized NAH (SONAH), Helmholtz Equation Least-Squares (HELS) or Inverse Boundary Element Method (IBEM).

4.1 Fourier-based NAH

The approaches to solve the inverse problem of NAH described in this section are based on the spatial Fourier transform. Although solutions for all separable coordinates systems are well-known [6], we focus only to the Cartesian and spherical coordinate systems to support the experiments performed for purposes of this thesis.

4.1.1 Planar NAH

In this section the basic acoustic equations in the Cartesian coordinates are briefly reviewed followed by the plane wave solution and the definition of the wavenumber space. Then the planar NAH is described.

4.1.1.1 Basic Acoustics Equations

In the Cartesian coordinates, $p(x, y, z, t)$ and $\mathbf{v}(x, y, z, t)$ stand for the space and time dependency of the acoustic pressure and particle velocity vector, respectively. Assuming the linear acoustic conditions, the acoustic pressure satisfies the wave equation

$$\nabla^2 p(x, y, z, t) - \frac{1}{c^2} \frac{\partial^2 p(x, y, z, t)}{\partial t^2} = 0, \tag{4.1}$$

where c is the speed of sound, $\partial^2/\partial t^2$ is the second partial derivative with respect to the time t and ∇^2 is partial differential operator defined as a sum of second partial derivatives with respect to the Cartesian coordinates. The particle velocity can be expressed using Euler's equation as

$$\rho_0 \frac{\partial \mathbf{v}(x,y,z,t)}{\partial t} = -\nabla p(x,y,z,t), \tag{4.2}$$

where ρ_0 is the air density and ∇ is the gradient defined as a vector composed of the first partial derivatives with respect to the Cartesian coordinates. Considering the harmonic functions and using the time-frequency Fourier transform[1] the time domain wave equation (4.1) could be transformed to the frequency domain, yielding the Helmholtz equation

$$\nabla^2 P(x,y,z,\omega) + k^2 P(x,y,z,\omega) = 0, \tag{4.3}$$

where $P(x,y,z,\omega)$ is the Fourier transform of the time domain acoustic pressure, $\omega = 2\pi f$ is the angular frequency (f is the frequency) and $k = \omega/c$ is the acoustic wave number. Similarly, the Euler's equation (4.2) in the frequency domain is

$$\mathrm{j}\omega\rho_0 \mathbf{V}(x,y,z,\omega) = \nabla P(x,y,z,\omega), \tag{4.4}$$

where $\mathbf{V}(x,y,z,\omega)$ is the particle velocity in the frequency domain and j is the imaginary unit.

4.1.1.2 Plane Waves and Wavenumber Space – k-space

The plane wave solution of Eq.(4.3) in three coordinates can be written [6] as

$$P(\omega) = A(\omega)\mathrm{e}^{\mathrm{j}(k_x x + k_y y + k_z z)} = A(\omega)\mathrm{e}^{\mathrm{j}\mathbf{k}\mathbf{r}}, \tag{4.5}$$

where $A(\omega)$ is an amplitude of acoustic pressure, $\mathbf{r} = (x,y,z)$ is the radius vector and $\mathbf{k} = (k_x, k_y, k_z)$ is the acoustic wavenumber vector, of which components satisfy the equality

$$k = |\mathbf{k}| = \sqrt{k_x^2 + k_y^2 + k_z^2}. \tag{4.6}$$

The acoustic wave-number vector determines the direction of propagation of the plane wave. For the description of radiation from planar sources, we will

[1] Time-Frequency Fourier Transform pair

$$F(\omega) = \int_{-\infty}^{\infty} f(t)\mathrm{e}^{-\mathrm{j}\omega t}\mathrm{d}t$$

$$f(t) = \frac{1}{2\pi}\int_{-\infty}^{\infty} F(\omega)\mathrm{e}^{\mathrm{j}\omega t}\mathrm{d}\omega$$

use the coordinate z emerging from the source surface lying on the x, y plane (the source surface is at $z_\mathrm{s} = 0$). As the wave number k is a constant at given frequency, we can choose one component of $\mathbf{k}$ dependent on the remaining two. For the purpose of dealing with the radiation from the planar sources, we have chosen k_z as a dependent component. Then, equation (4.6) yields

$$k_z = \pm\sqrt{k^2 - k_x^2 - k_y^2}, \tag{4.7}$$

where the independent components k_x and k_y could take arbitrary real values. Hence, two situations can occur. First, when $k^2 \geq k_x^2 + k_y^2$ and choosing the positive sing in Eq.(4.7), the component k_z will be a positive real number that physically represents the plane wave (described by Eq. (4.5)) propagating in direction given by $\mathbf{k}$ without any dissipation (when neglecting the loss of energy due to the propagation in the air, which is a correct assumption in the near field). Second, when $k^2 < k_x^2 + k_y^2$, Eq.(4.7) can be express as

$$k_z = \pm\sqrt{k^2 - k_x^2 - k_y^2} = \pm\mathrm{j}k_z^+, \tag{4.8}$$

where k_z^+ is a positive real number. According to the Sommerfeld radiation condition[2] only the positive sign is physically correct in this case. After substitution to Eq.(4.5), we can write

$$P(\omega) = A(\omega)\mathrm{e}^{\mathrm{j}(k_x x + k_y y)}\mathrm{e}^{-k_z^+ z}. \tag{4.9}$$

The equation (4.9) represents the waves that exponentially decay with distance from the source surface. Such waves are commonly called evanescent waves in the literature. An attenuation of these waves is caused by the hydrodynamic short circuit that almost cancels out the radiation from areas with opposite phase due to the destructive interferences. Hence, these waves do not radiate to the far field and can be measured only in the near field of the source. As we will show in the latter section dealing with the sound radiation by thin plates, the wavelengths $\lambda = c/f$ of evanescent waves travelling along the source surface are shorter than the corresponding wavelengths in the air. Therefore, the reconstruction of these waves increases the resolution – their capturing is very important and fundamental for NAH.
On the basis of the Eq.(4.7) an analysis of sound radiation could be carried out in the wavenumber domain, which is usually called k-space in the literature. A quantity defined in the space domain can be transformed to the k-space (and vice versa) using two-dimensional Fourier transform pair[3]. The k-space

[2] Sommerfeld radiation condition prescribes the boundary condition at infinity. Therefore the positive sign ensures the attenuation of waves.

$$\lim_{\mathbf{r}\to\infty} r\left[\frac{\partial}{\partial r} - \mathrm{j}k\right] p(\mathbf{r}) = 0$$

[3] Space-Wavenumber domain Fourier Transform pair

$$F(k_x, k_y) = \int_{-\infty}^{\infty}\int_{-\infty}^{\infty} f(x,y)\mathrm{e}^{-\mathrm{j}(k_x x + k_y y)}\mathrm{d}x\mathrm{d}y$$

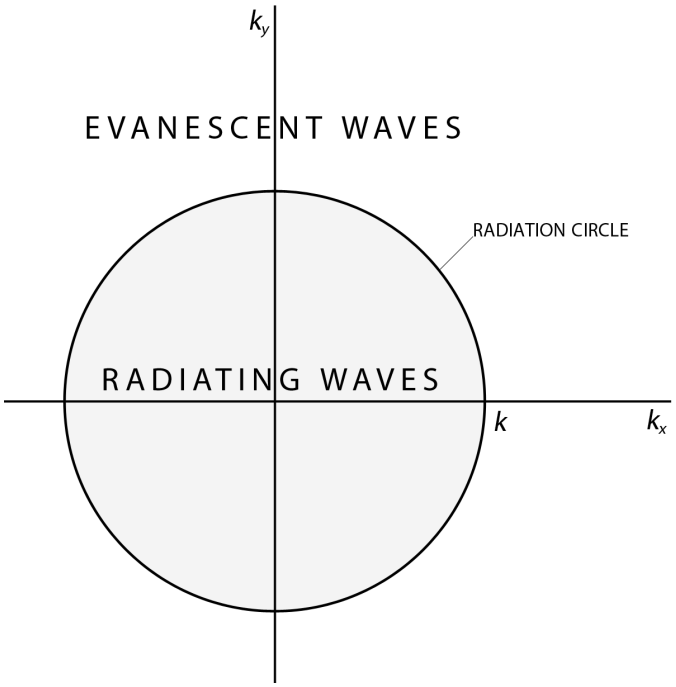

Figure 4.1: k-space

is shown in Fig.4.1 together with the circle of radius equal to k (the radiation circle) dividing the space into two areas. The plane waves propagating to the far field belong inside the area inside the circle, whereas the evanescent waves belong to the external area. According to the wave speed $c = \omega/k$, the internal area includes the "structural" waves (the bending waves in a plate) traveling at the speed greater than the speed of waves in the air, whereas the external area includes the slower ones. Hence, the labels supersonic and subsonic area, respectively, can regularly be found in the literature [6]. The sound pressure $p(x, y, z = z_\mathrm{h})$ on some two-dimensional plane at $z = z_h$ could be using two-dimensional Fourier transform expressed in the k-space as

$$P(k_x, k_y, z_\mathrm{h}) = \int_{-\infty}^{\infty}\int_{-\infty}^{\infty} p(x, y, z_\mathrm{h})\mathrm{e}^{-\mathrm{j}(k_x x + k_y y)}\mathrm{d}x\mathrm{d}y. \tag{4.10}$$

$$f(x, y) = \int_{-\infty}^{\infty}\int_{-\infty}^{\infty} F(k_x, k_y)\mathrm{e}^{\mathrm{j}(k_x x + k_y y)}\mathrm{d}k_x\mathrm{d}k_y$$

4.1.1.3 Forward Problem

Rewriting the first Rayleigh integral formula (Eq. (2.13)) for known pressure at a plane $z = z_\mathrm{h}$ yields

$$p(x, y, z) = \int_{-\infty}^{\infty} \int_{-\infty}^{\infty} p(x_\mathrm{h}, y_\mathrm{h}, z_\mathrm{h}) G_\mathrm{D}(x - x_\mathrm{h}, y - y_\mathrm{h}, z - z_\mathrm{h}) \,\mathrm{d}x_\mathrm{h} \,\mathrm{d}y_\mathrm{h}. \quad (4.11)$$

This equation represents the convolution of two-dimensional acoustic pressure and propagator function satisfying Dirichlet's boundary condition and provides a tool for computation of the acoustic pressure on a plane at a distance $z - z_\mathrm{h}$. Symbolically the equation can be written in a compact form as

$$p(x, y, z) = p(x_\mathrm{h}, y_\mathrm{h}, z_\mathrm{h}) * G_\mathrm{D}(x - x_\mathrm{h}, y - y_\mathrm{h}, z - z_\mathrm{h}). \quad (4.12)$$

For $z - z_\mathrm{h} \geq 0$ the above stated equations represent the forward problem and provide the acoustic pressure computation on a plane further from the sound source. Using the k-space formulation, the Eq. (4.11) (resp. (4.12)) can be stated as

$$P(k_x, k_y, z) = P(k_x, k_y, z_\mathrm{h}) \cdot G_\mathrm{D}(k_x, k_y, z - z_\mathrm{h}), \quad (4.13)$$

where the acoustic pressure propagator function

$$G_\mathrm{D}(k_x, k_y, z - z_\mathrm{h}) = \mathrm{e}^{\mathrm{j}k_z(z - z_\mathrm{h})}. \quad (4.14)$$

In an analogous way based on the second Rayleigh integral formula (Eq. (2.14)) a computation of the normal component of particle velocity can be expressed using the velocity propagator function satisfying Neumann's boundary condition as

$$V_\mathrm{n}(k_x, k_y, z) = P(k_x, k_y, z_\mathrm{h}) \cdot G_\mathrm{N}(k_x, k_y, z - z_\mathrm{h}), \quad (4.15)$$

where

$$G_\mathrm{N}(k_x, k_y, z - z_\mathrm{h}) = \frac{k_z}{\rho_0 c k} \mathrm{e}^{\mathrm{j}k_z(z - z_\mathrm{h})}. \quad (4.16)$$

Note that for the forward problem the exponential part in Eq. (4.14) and Eq. (4.16) performs a phase change of the plane propagating waves and an exponential decay of the evanescent waves as described in the previous section.

4.1.1.4 Inverse Problem

Inversion of the equation representing the forward problem is an essential idea of the NAH. This inversion could be represented using the condition $z - z_\mathrm{h} \leq 0$ for the planar Fourier-based NAH. A computation of the acoustic pressure and/or particle velocity is commonly termed as a reconstruction concerning the inverse problem symbolizing the inverse time computation. Therefore,

the acoustic pressure (resp. particle velocity) can be reconstructed on a plane at a distance closer to a sound source then the measurement (holographic) plane at $z = z_\mathrm{h}$ using Eq. (4.13) (resp. (4.15)). In this case the exponential exponential part in the propagator functions performs a phase change of the plane propagating waves and exponential amplification of the evanescent waves. Precise filtering of these waves is crucial for correct reconstruction.

4.1.1.5 Limitations and resolution

This approach suffers from the limited aperture size restricting the integration bounds in the spatial Fourier transform. Therefore, the aperture size need to be at least four times as large (two times in both directions) as a source surface. On the other hand the resolution (the highest frequency that could be reconstructed) depends on a mutual distance of the sampling points (in case of regular sampling grid) – according to the Nyquist-Shannon sampling theorem. This makes the approach very impractical requiring a huge number of sampling points even for relatively small sound sources or large measurement time in case of scanning the measurement grid assuming stationary sound field. Apart from the fast Fourier transform implementation applicability, the computational complexity is increased due to a large number of points. There are several techniques (such as Patch-NAH, see [4],[11] and [10]) as well as different approaches (such as SONAH and HELS described in the latter sections) dealing with overcoming this limitation.

4.1.2 Spherical NAH

In this section, a processing based on the spherical harmonics decomposition is briefly reviewed and subsequently focused on the performance in the near-field of an array. The description of the forward problem in a spherical coordinates system is stated followed by its inversion representing the spherical NAH. A graphic illustration of the exterior and interior domain is depicted in Fig. 4.2. In this figure the surface of a sphere on which the acoustic quantity(ies) is known is described using the radius r_h, a sphere on which the acoustic quantity(ies) could be calculated is described using the radius r satisfying $r_\mathrm{min} \leq r \leq r_\mathrm{max}$. The hatched parts illustrate the regions of the inverse problem.

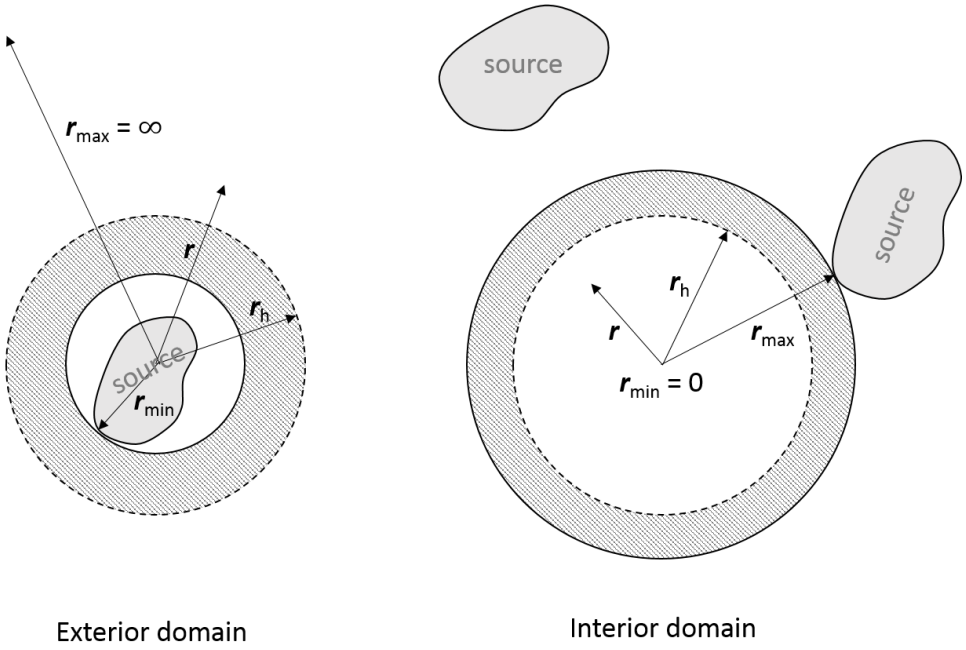

Figure 4.2: Exterior and interior domain for forward and inverse spherical problem

4.1.2.1 Spherical Harmonics Decomposition

The wave equation in spherical coordinates is

$$\frac{1}{r^2}\frac{\partial}{\partial r}\left(r^2\frac{\partial p}{\partial r}\right)+\frac{1}{r^2\sin\theta}\frac{\partial}{\partial\theta}\left(\sin\theta\frac{\partial p}{\partial\theta}\right)+\frac{1}{r^2\sin^2\theta}\frac{\partial^2 p}{\partial\phi^2}=\frac{1}{c^2}\frac{\partial^2 p}{\partial t^2}, \tag{4.17}$$

where $r=\sqrt{x^2+y^2+z^2}$, $\theta=\tan^{-1}(\sqrt{x^2+y^2}/z)$ and $\phi=\tan^{-1}(y/x)$ are the spherical coordinates. The solution of Eq.(4.17) could be found for separate variables r,θ,ϕ and t. The solution for angular functions θ and ϕ leads to the spherical harmonics defined as

$$Y_n^m(\theta,\phi)=\sqrt{\frac{(2n+1)}{4\pi}\frac{(n-m)!}{(n+m)!}}P_n^m(\cos\theta)\mathrm{e}^{\mathrm{j}m\phi}, \tag{4.18}$$

where the integer numbers n and m represent the order and degree ($m\in[-n,n]$), respectively, of corresponding spherical harmonic and $P_n^m(\cos\theta)$ are the (associated) Legendre functions [6]. The spherical harmonics, depicted in Fig. 4.3 constitute the orthonormal basis for the spherical Fourier transform.

The acoustic pressure on the surface of a sphere of radius $r=r_\mathrm{h}$ can be described by the coefficients $P_{mn}(r_\mathrm{h})$ of the spherical harmonics using the spherical Fourier transform

$$P_{mn}(r_\mathrm{h})=\int_0^{2\pi}\int_0^{\pi}p(r_\mathrm{h},\theta,\phi)Y_n^{m*}(\theta,\phi)\sin\theta\mathrm{d}\theta\mathrm{d}\phi, \tag{4.19}$$

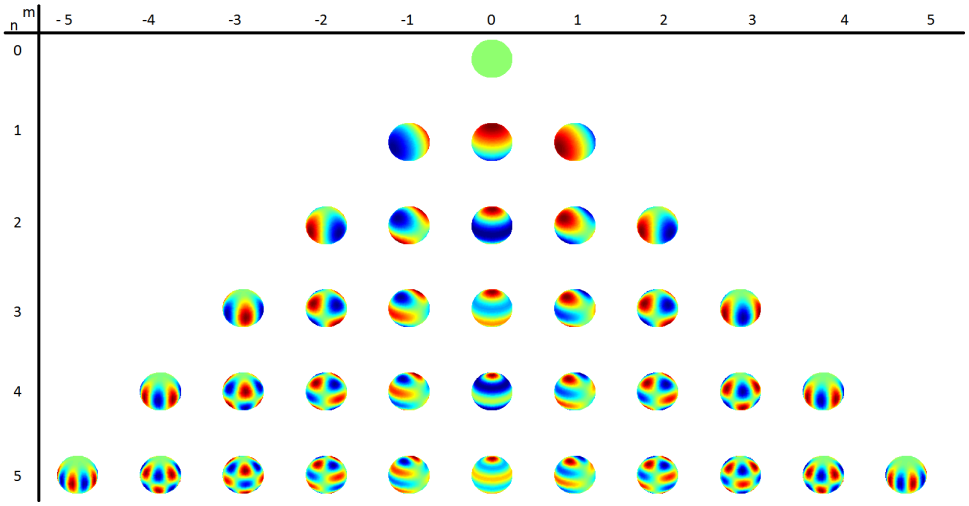

Figure 4.3: Spherical harmonics

where the integration is performed over the entire sphere and the asterisk stands for the complex conjugation. The inverse Fourier transform is then simply

$$p(r_\mathrm{h},\theta,\phi) = \sum_{n=0}^{\infty}\sum_{m=-n}^{n} P_{mn}(r_\mathrm{h})Y_n^m(\theta,\phi). \tag{4.20}$$

Note that in real application the acoustic pressure is acquired at a finite number of points over a sphere, so $p(r_\mathrm{h},\theta_l,\phi_l)$ for $l = 1,\ldots,L$, where L is the total number of points. The total number of (sampling) points as well as their distribution over the sphere is critical for correct numerical evaluation of Eq.(4.19) and determines the maximum order $n = N$ of the spherical harmonics Y_n^m that could be used in processing without any aliasing effect (considering the surrounding sound field to be harmonics-order limited, $P_{mn} = 0 : \forall n > N$). Finite number of sampling points limits the infinite summation in Eq. (4.20) and discretizes the integration in Eq. (4.19). The error caused by this limitation is usually termed the *base system error* and diminishes to zero as N increases to infinity [34]. The topic of distributing the sampling points over a sphere is very broad and even if it is critical for real application of the spherical NAH it is not discussed in depth exceeding the scope of this thesis – interested reader could find more information in referred publications such as [23, 27, 28, 29, 30] and consequent bibliographies.

4.1.2.2 Radial Dependence

The solution for radial dependence variable r leads to the spherical Bessel functions of the third kind (spherical Hankel functions)

$$h_n(kr) = j_n(kr) \pm \mathrm{j}y_n(kr), \tag{4.21}$$

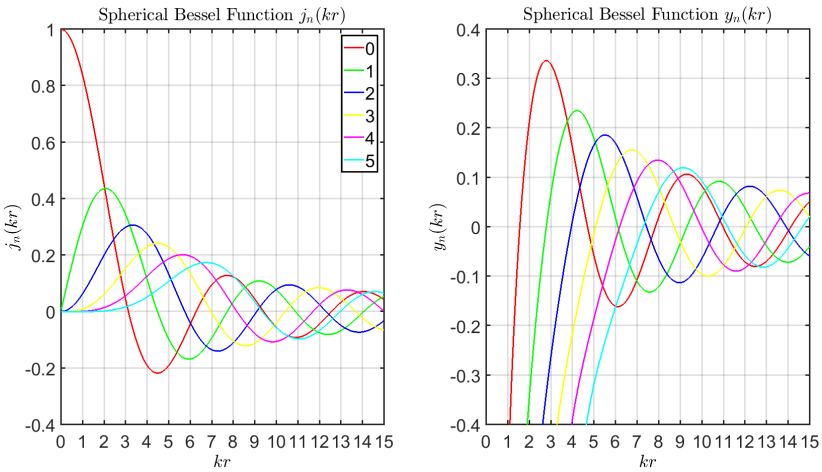

Figure 4.4: The Bessel functions of the first and second kind

where n is the order of the function and $j_n(kr)$ and $y_n(kr)$ are the spherical Bessel functions of the first and second kind, respectively, and could be expressed using corresponding Bessel functions (J_n, Y_n) such as

$$\begin{aligned} j_n(kr) &= \sqrt{\frac{\pi}{2kr}} J_{n+1/2}(kr) \\ y_n(kr) &= \sqrt{\frac{\pi}{2kr}} Y_{n+1/2}(kr). \end{aligned} \tag{4.22}$$

The sign in Eq. (4.21) corresponds to the wave propagation orientation (it is equivalent to the choice of sign for the plane wave propagation in the space described using $\mathrm{e}^{\pm \mathrm{j}kr}$ or in the time described using $\mathrm{e}^{\pm \mathrm{j}\omega t}$). Therefore, while the plus sign in Eq. (4.21) represents an outgoing spherical wave (the forward problem), the minus sign represents an incoming spherical wave (the inverse problem). The Bessel functions of the first and second kind are depicted in Fig. 4.4.

4.1.2.3 Forward Problem

Consider the acoustic pressure to be known (e.g . measured) on a surface of a sphere of radius $r = r_\mathrm{h}$ and described using the spherical harmonics coefficients $P_{mn}(r_\mathrm{h})$. For the exterior domain, the coefficients of acoustic pressure in a region $r \geq r_\mathrm{h}$ can be calculated as

$$P_{mn}(r) = \frac{h_n(kr)}{h_n(kr_\mathrm{h})} P_{mn}(r_\mathrm{h}) \tag{4.23}$$

and using the Euler equation (while considering a derivative in the radial direction) the coefficients of radial particle velocity can be calculated as

$$V_{r,mn}(r) = \frac{1}{\mathrm{j}\rho_0 c}\frac{h_n^{'}(kr)}{h_n(kr_\mathrm{h})}P_{mn}(r_\mathrm{h}). \tag{4.24}$$

For the interior domain the coefficients of acoustic pressure in a region $r \leq r_\mathrm{h}$ can be calculated in a similar way as

$$P_{mn}(r) = \frac{j_n(kr)}{j_n(kr_\mathrm{h})}P_{mn}(r_\mathrm{h}) \tag{4.25}$$

and the coefficients of particle velocity as

$$V_{r,mn}(r) = \frac{1}{\mathrm{j}\rho_0 c}\frac{j_n^{'}(kr)}{j_n(kr_\mathrm{h})}P_{mn}(r_\mathrm{h}). \tag{4.26}$$

A detailed derivation of these equations could be found in [6] together with tangential components of particle velocity as well as the calculation of the acoustic pressure based on the known particle velocity on the surface $r = r_\mathrm{h}$.

4.1.2.4 Inverse Problem

The inverse problem constituted by the NAH tries to solve the acoustic field in a region depicted using a hatched volume in Fig. 4.2. For the exterior domain this region is defined by $r_\mathrm{min} \leq r \leq r_\mathrm{h}$, while for the interior domain by $r_\mathrm{h} \leq r \leq r_\mathrm{max}$. The equations Eqs. (4.23-4.26) stated for the forward problem are still valid when considering their application in these regions.
As has been mentioned, reconstruction of the acoustic quantities in direction towards the sound source(s) is the ill-posed problem due to the amplification of the evanescent waves contaminated by the noise. This amplification is evident by the behavior of acoustic transfer function for $kr_\mathrm{h} \ll n$. It can be shown that for exterior domain the transfer function

$$\frac{h_n(kr)}{h_n(kr_\mathrm{h})} \approx \left(\frac{r_\mathrm{h}}{r}\right)^{n+1} \tag{4.27}$$

and for the interior domain the transfer function

$$\frac{j_n(kr)}{j_n(kr_\mathrm{h})} \approx \left(\frac{r}{r_\mathrm{h}}\right)^{n}. \tag{4.28}$$

4.1.2.5 Near-field Spherical Microphone Array Processing

The transition between the near and far field of an array is usually related to the approximation error of spherical wavefront in relation to the plane wave.

Therefore, in the case of the capability of an array to capture the spherical wavefront, such information could be advantageously utilized. As expected, the array near field capabilities depend on its design as well as the processing frequency. The radial processing focusing on this close region of an array is reviewed in this section. In designing the spherical microphone array, the critical parameters influencing its spatial resolution are the total number of the microphones spatially sampling the surrounding sound field, as well as their distribution around the sphere surface.

To evaluate the near-field information, the plane wave (generated by a source at infinity – in the far field) and spherical wave (generated by a source in the near field of an array) impinging the measurement sphere are to be studied separately. Two types of the measurement sphere are usually considered depending on its scattering properties of an incidenting sound field – open and rigid sphere. The corresponding Fourier coefficients can be expressed as [26]

$$P_{mn}(r_\mathrm{h},\omega) = \begin{cases} b_n(k,r)Y_n^{m*}(\theta_0,\phi_0), & \text{for plane wave,} \\ b_n^s(k,r,r_\mathrm{s})Y_n^{m*}(\theta_\mathrm{s},\phi_\mathrm{s}), & \text{for spherical wave,} \end{cases} \tag{4.29}$$

where (θ_0,ϕ_0) represent the direction of propagation of the plane wave, $(r_\mathrm{s},\theta_\mathrm{s},\phi_\mathrm{s})$ represent the location of point source and k is the wavenumber. The so called *far-field mode-strength function* $b_n(k,r)$ derived for an open and rigid sphere considering the plane wave impinging the sphere can be expressed as

$$b_n(kr) = 4\pi\mathrm{j}^n \begin{cases} j_n(kr) & \text{for open sphere,} \\ j_n(kr) - \dfrac{j_n^{'}(kr_\mathrm{h})}{h_n^{'}(kr_\mathrm{h})}h_n(kr) & \text{for rigid sphere.} \end{cases} \tag{4.30}$$

The prime stands for the derivative with respect to the argument. While the rigid sphere influences the surrounding sound field by its acoustically hard surface (zero surface velocity), the open sphere is considered acoustically transparent and do not influence the sound field.
On the contrary, assuming the point source located in the near-field of an array (a spherical wave impinging the sphere), the analogous *near-field mode-strength function* is

$$b_n^\mathrm{s}(k,r,r_\mathrm{s}) = \mathrm{j}^{-(n-1)}kb_n(kr)h_n(kr_\mathrm{s}). \tag{4.31}$$

By exploring Eq. (4.31) (using $b_n(kr)$ for the open and rigid sphere defined in Eq. (4.30)) it is clear that the spherical wave behavior is embodied by the function $h_n(kr_\mathrm{s})$. By comparison of both plane and spherical mode-strength functions, the near field criterion can be expressed as

$$r_\mathrm{NF} \approx \frac{N}{k}. \tag{4.32}$$

In this region, the possibility of capturing spherical wavefront by an array can be assumed. Note the dependency on array design hidden in the maximal order N and dependency on frequency, as mentioned earlier. Determination of the distance $r_\mathrm{s} \leq r_\mathrm{NF}$ is the subject of the next section.

4.1.2.6 Source distance determination

In this section, the determination of the distance r_s based on the spherical Fourier coefficients of the measured pressure is described. The motivation of such an approach is given by the possibility of distance determination in situations, in which the direct measurement by mechanical or optical meter is impractical and/or complicated. Starting with the simple determination of distance of the static point source, this approach can find its usability in case of the point-like source moving in the near field of an array. Moreover, the generalization of this method for more complicated and/or multiple sources including the source separation processing techniques is the subject of further research.
The *overall spherical wave mode-strengths* can be calculated for all possible spherical modes (the orders n of spherical harmonics) from the Fourier coefficients (Eq. (4.29)) of all respective degrees $m \in [-n, n]$ as

$$\sum_{m=-n}^{n} |P_{mn}|^2 = \frac{(2n+1)}{4\pi} |b_n^\mathrm{s}(k, r, r_\mathrm{s})|^2, \tag{4.33}$$

utilizing the equality

$$\sum_{m=-n}^{n} |Y_n^m(\theta, \phi)|^2 = \frac{(2n+1)}{4\pi}.$$

Eq. (4.33) represents the overall strength of the corresponding spherical mode of order n. The determination is based on the division of two adjacent mode-strengths

$$\begin{aligned} \frac{\sum_{m=-n}^{n} |P_{m,n+1}|^2}{\sum_{m=-n}^{n} |P_{mn}|^2} &= \frac{(2n+3)|b_{n+1}^\mathrm{s}(k, r, r_\mathrm{s})|^2}{(2n+1)|b_n^\mathrm{s}(k, r, r_\mathrm{s})|^2} = \\ &= \frac{(2n+3)|b_{n+1}(kr)h_{n+1}(kr_\mathrm{s})|^2}{(2n+1)|b_n(kr)h_n(kr_\mathrm{s})|^2}. \end{aligned} \tag{4.34}$$

The derivation is first presented in the case without any approximation of the radial functions, and then with the approximation valid for the low frequency assumption.

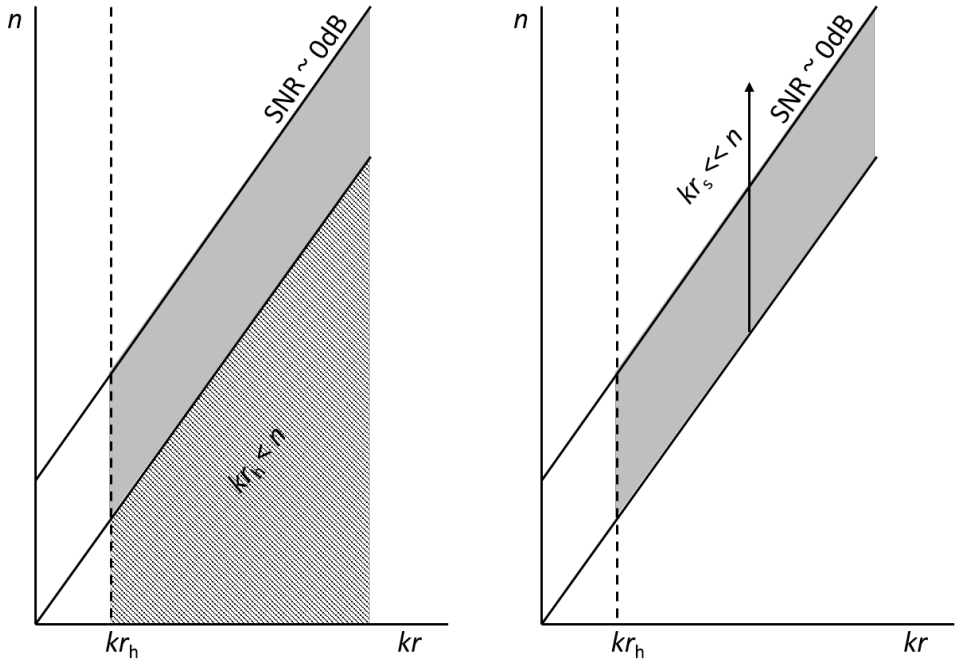

Figure 4.5: Regions of applicability. Left: no-approximation method, the region of applicability is depicted by hatched together with shaded area. Right: with low-frequency approximation, the region of applicability is depicted by shaded area

4.1.2.7 No approximation

By dividing two adjacent mode strengths (see Eq. (4.34)) and expressing for the distance-dependent functions, one can obtain the equation

$$\frac{|h_{n+1}(kr_\mathrm{s})|^2}{|h_n(kr_\mathrm{s})|^2} = \frac{(2n+1)|b_n(ka)|^2 \sum_{m=-(n+1)}^{n+1} |P_{m,n+1}|^2}{(2n+3)|b_{n+1}(ka)|^2 \sum_{m=-n}^{n} |P_{m,n}|^2}. \tag{4.35}$$

While the left-hand side of Eq. (4.35) is exponentially decaying with respect to the argument, the right hand side is a constant for the given configuration (a, n, k). Therefore, finding the equality of both sides leads to the determination of the distance to the origin of a spherical wave. Although it is possible to use an arbitrary value of n for the determination, the maximum order is always subject to the signal-to-noise ratio. The nature of the coefficients of spherical harmonics has already been discussed in section 4.1.2.4, in which the rapid decay of the coefficients while $n \ll k$ has been demonstrated. This behavior is also obvious in our model validation. In the left part of Figure 4.5, the area of applicability of this method is shown (hatched together with shaded) depending on the order n of spherical harmonics and kr. Note that the above-mentioned condition for the coefficients is not as strict, and is represented by the upper diagonal line (SNR $\approx 0\,$dB). Those coefficients that

are above the noise level are still usable for the determination. Therefore, the applicability of this method is limited for higher orders, whose coefficients are significantly influenced by the noise.

4.1.2.8 Low-frequency approximation

Considering $kr_\mathrm{s} << n$, it is possible to approximate spherical radial functions (j_n and h_n) and extract the distance r_s. Again, by dividing two adjacent mode strengths (see Eq. (4.34)) and using the approximations [6]

$$\frac{|h_{n+1}(kr_\mathrm{s})|}{|h_n(kr_\mathrm{s})|} \approx \frac{2n+1}{kr_\mathrm{s}} \tag{4.36}$$

and

$$\frac{|b_{n+1}(ka)|}{|b_n(ka)|} \approx \frac{ka(n+1)}{(2n+1)(n+2)}, \tag{4.37}$$

the latter being valid for the rigid sphere (not for the open sphere), the distance to the origin of a spherical wave can be extracted and expressed as

$$r_\mathrm{s} = a\sqrt{\frac{(2n+3)(n+1)^2\sum_{m=-n}^{n}|P_{m,n}|^2}{(2n+1)(n+2)^2\sum_{m=-(n+1)}^{n+1}|P_{m,n+1}|^2}}. \tag{4.38}$$

In a similar way, the area of applicability is shown in the right part of Figure 4.5. In this case, the consideration used for approximation restricts the usable coefficients to only those satisfying both conditions.

4.2 Least-squares NAH

The two methods described in this section have been developed to overcome the aperture size limitations valid for the Fourier-based NAH. These methods use the elementary wave model (EWM) to approximate the measured acoustic quantity. The EWM could be composed of any functions and its definition usually corresponds with the geometry of the sound source(s) as well as the geometry of the measurement aperture (to be able to represent any acoustic field, the EWM should constitute a complete basis).
Consider the acoustic pressure $p(\mathbf{r}_{\mathrm{h},i})$ to be measured in some (reasonable) points in space defined by the position vectors $\mathbf{r}_{\mathrm{h},i}$. The expansion of measured pressure into the EWM is described as

$$p(\mathbf{r}_{\mathrm{h},i}) = \sum_{n=1}^{N} c_n\psi_n(\mathbf{r}_{\mathrm{h},i}), \tag{4.39}$$

where $c_n \in \mathbb{C}$ are the expansion coefficients and the maximal order $n = N$ should avoid the aliasing effects – the total number of measurement points as well as their distribution should ensure that the measured acoustic field is sampled according to the Shannon theorem. The matrix formulation of the Eq. (4.39) could be written as

$$\mathbf{p} = \psi_\mathrm{h}\mathbf{c}, \tag{4.40}$$

where matrix $\psi_\mathrm{h} \in \mathbb{C}^{L\times N}$ contains all the elementary wave functions (columns) evaluated in all the measurement points (rows) and the vectors $\mathbf{p} \in \mathbb{C}^{L\times 1}$ and $\mathbf{c} \in \mathbb{C}^{N\times 1}$ contain measured pressures and expansion coefficients, respectively. When $L \geq N$ the regularized solution of the over-determined system of linear equations in Eq. (4.40) could be written as

$$\mathbf{c} = (\psi_\mathrm{h}^\mathrm{H}\psi_\mathrm{h} + \alpha\mathbf{I})^{-1}\psi_\mathrm{h}^\mathrm{H}\mathbf{p}. \tag{4.41}$$

The expansion coefficients in the matrix $\mathbf{c}$ relates the elementary wave model functions and acoustics quantity at the measurement positions. Using these coefficients, these functions can be evaluated in the positions everywhere in regions valid for external and internal domain for both forward and inverse problems.

4.2.1 SONAH – Statistically Optimized NAH

Statistically Optimized NAH (SONAH) has been developed by Steiner and Hald [42] to overcome the limitations that are caused by the use of the Fourier transform (it completely avoids this spatial-wavenumber transform). It considers a series of propagating plane and evanescent waves as eigen-functions, that represent separable solution of Helmholtz equation (see section 4.1.1.2). The acoustic pressure on the source surface $p(\mathbf{r}_\mathrm{s})$ (generally everywhere in the space) can be expressed as a weighted sum of the measured pressure $p(\mathbf{r}_\mathrm{h})$ in the space [16]

$$p(\mathbf{r}_\mathrm{s}) = \sum_{n=1}^{N} c_n p(\mathbf{r}_\mathrm{h}) \quad \longrightarrow \quad \mathbf{p}(\mathbf{r}_\mathrm{s}) = \mathbf{p}^T(\mathbf{r}_\mathrm{h})\mathbf{c}, \tag{4.42}$$

where T represents the matrix (vector) transpose. The vector $\mathbf{c}$ (respective the weight coefficients c_n) is computed as a least-squares solution of the functions determined at points in the space $\mathbf{A}(\mathbf{r}_\mathrm{h})$ and on the source surface $\alpha(\mathbf{r}_\mathrm{s})$ (matrices containing all functions for each position in the space and on the source surface, respectively). Thus, it consists of functions depending only on the relative positions of those points. The acoustic pressure on the source surface can be formulated as

$$p(\mathbf{r}_\mathrm{s}) = \mathbf{p}^T(\mathbf{r}_\mathrm{h})(\mathbf{A}^H\mathbf{A} + \lambda^2\mathbf{I})^{-1}\mathbf{A}^H\alpha(\mathbf{r}_\mathrm{s}) \tag{4.43}$$

where λ is the regularization parameter, $\mathbf{I}$ is the identity matrix and H represents the Hermitian transpose of a matrix.
SONAH is an approximate method and the reconstruction may diverge even without noise. A discretization of k-space must be performed carefully to ensure correct approximation. Jacobsen and Hald extend this method for the pressure-velocity sensors measurement, which shows better results for the normal surface velocity reconstruction from particle velocity measurement and provides some possibilities to control the sound waves coming from other directions [16]. For this purpose, several papers also deal with the two-layer arrays [18].

4.2.2 HELS – Helmholtz Equation Least Squares

The Helmholtz Equation Least-Squares has been developed by Wang and Wu [8]. The main idea is to interpolate measured pressures by the spherical harmonic functions

$$\psi_{mn}(r,\theta,\phi) = h_m(kr)P_n^m(\cos\theta)\exp(\mathrm{j}m\phi) \tag{4.44}$$

where $h_m(kr)$ is the spherical Hankel function and P_n^m is the Legendre polynomials. These functions satisfy the Helmholtz equation. Before interpolation the functions are orthonormalized using the Gramm-Schmidt algorithm. The coefficients of linear combination of functions ψ at the measurement points are calculated using the least-squares method which leads to

$$\mathbf{c} = (\rho c)^{-1}(\mathbf{B}^H\mathbf{B} + \lambda\mathbf{I})^{-1}\mathbf{B}^H\mathbf{p}. \tag{4.45}$$

Matrix $\mathbf{B}$ contains in each row N spherical harmonics used to interpolate pressure in one measurement point. Reconstructed pressures $\mathbf{p}_s$ at selected points are given by

$$\mathbf{p}_\mathrm{s} = \mathbf{B}_\mathrm{s}\mathbf{c} \tag{4.46}$$

where $\mathbf{B}_s$ is the matrix consisting of spherical harmonics as in matrix $\mathbf{B}$ but in points where the pressure should be reconstructed.
This method is also the approximation method suitable primarily for the convex surfaces. The number of expansion functions is crucial for the correct approximation. For both SONAH and HELS, the number of measurement points need not be as high as for the Fourier-based NAH, but generally, the more the measurement points, the better the approximation.

Part II

Practical Part

Chapter 5

Experiments

In this chapter, the results of simulations as well as practical experiments are presented. Individual chapters contain parts of the papers published during the author's doctoral study. The resulting graphic presentations are stated in appendices. Corresponding references are stated in the beginning of each chapter.

5.1 Near-field Acoustic Holography Based on Combined Elementary Wave Model

Reconstruction of sound field sources distribution using Nearfield Acoustic Holography (NAH) based on elementary wave models (EWM) was presented in paper [43]. The commonly used models include planar (SONAH) cylindrical or spherical (HELS) waves. In our approach we decide to use a combination of these models according to frequency and measured aperture size. Also different k-space sampling methods were tested. The comparison was done firstly on the model data set and subsequently on the real measurement data and the accuracy of reconstructions was compared. Direct measurement of normal surface velocity with a laser scanning vibrometer was performed in order to objectively evaluate the results.

5.1.1 Combined Elementary Wave Model

The combined EWM method uses linear combination of pre-selected expansion functions to interpolate measured pressures. These functions are solutions of the Helmholtz equation in a source free region. In matrix formulation we can write

$$\mathbf{Bc} = \mathbf{p} \tag{5.1}$$

where $\mathbf{B} = \{\psi(\mathbf{r}_i)\}$ is the matrix consisting of expansion functions ψ at measurement points $\mathbf{r}_i$, $\mathbf{p}$ represents measured complex pressures and $\mathbf{c}$ is vector of coefficients in linear combination. Assuming least-squares solution of (5.1) using standard Tikhonov regularization, one may express the solution for $\mathbf{c}$ as

$$\mathbf{c} = (\mathbf{B}^H\mathbf{B} + \alpha\mathbf{I})^{-1}\mathbf{B}^H\mathbf{p}. \tag{5.2}$$

The sound pressure $\mathbf{p}_s$ at points on the source is then calculated as a linear combination of elementary expansion functions in these points (described by matrix $\mathbf{B}_s = \{\psi(\mathbf{r}_s)\}$) multiplied by weight vector $\mathbf{c}$

$$\mathbf{p}_s = \mathbf{B}_s\mathbf{c}. \tag{5.3}$$

In the combined elementary wave model we use plane wave solutions (described in SONAH, see chapter 4.2.1) as well as spherical harmonics (described in HELS, see chapter 4.2.2) as basis functions. In addition, any other suitable solutions of the Helmholtz equation may be selected according to source geometry.

5.1.2 Experiment

The reconstruction by combined EWM was first verified on an imaginary source that was generated for several typical surface geometries as a linear combination of planar and spherical functions with certain coefficients. After that this method was applied to the reconstruction of an acoustic pressure field on a real source surface.

The rectangular steel plate fixed in corners of dimensions $1 \times 0.7 \times 0.002\,\mathrm{m}$ was excited by a random force at a single fixed point on the structure ($x = 0.3\,\mathrm{m}$, $y = 0.17\,\mathrm{m}$). As an excitation signal band noise $100 - 3000\,\mathrm{Hz}$ was used. The normal velocity measured by a laser scanning vibrometer served as a reference for the reconstructed images. The complex pressures were measured $0.015\,\mathrm{m}$ above the surface in a grid of 24×19 points.

5.1.3 Experimental results

All three methods described above to reconstruct sound pressure distribution at the planar source surface for two selected frequency bands were tested. These bands were chosen according to the mean spectrum of the signals from all microphones. Reconstruction of an acoustic pressure on the source plane for the first frequency band, 508-512 Hz, for each method is shown in Fig. A.1 together with the pressure computed using Euler's equation from measured normal surface velocities by the laser scanning vibrometer. The number of functions used for reconstruction is for each method also specified. The number $N_s = 625$ (for SONAH) corresponding to 25 samples for each independent component of wave number (k_x,k_y). The number $N_h = 351$ (for HELS) is determined by the order(s) and degree of spherical harmonics (25th degree and all appropriate orders in this case). For the combined EWM these numbers denotes the number of the most significant functions taken from each model. In order to evaluate the results the source plane was divided into the several small parts (six in x direction and four in y direction) in which the relative errors in reference to the laser pressures were computed. These errors are for the first band shown in a chart in Fig. A.3. Mean errors for each method are $E_{\text{sonah}} = 0.29$, $E_{\text{hels}} = 0.38$ and $E_{\text{comb}} = 0.35$. Results of reconstruction for second band, 176-178 Hz are similarly shown in Fig. A.2 and Fig. A.4. Mean errors for each method are $E_{\text{sonah}} = 0.36$, $E_{\text{hels}} = 0.45$ and $E_{\text{comb}} = 0.39$.

5.1.4 Conclusions

Within this experiment three methods for reconstruction of sound pressure at the source surface from data measured in the near-field were compared. The combined elementary wave model method was compared with results of other two well-known and established methods – SONAH and HELS. As basis functions for the combined EWM algorithm were selected plane wave and evanescent functions from SONAH and also spherical harmonics from HELS. By appropriate selection of used functions we achieve similar results (with comparable error and resolution) while the number of basis functions was significantly reduced. The method was tested on model data as well as on real measurement data. As a reference for all tested methods a laser scanning vibrometer measurement was used. From measured normal velocity distribution we calculate the sound pressure distribution on the source surface. Several new parameters arising from combining different basis functions affect the reconstruction results. A priori selection of the best-fit functions could reduce the computational complexity while maintaining a good accuracy.

5.2 Reconstruction of normal surface velocity from measurement of acoustically induced vibration of a thin membrane

The theoretical study of extension of the laser scanning vibrometer measurement for reconstruction of acoustic quantities by Nearfield Acoustical Holography (NAH) were presented in paper [44]. This approach could be applied in a situation where the direct measurement of source vibration is complicated or impossible. A thin rectangular membrane with reflective coating is inserted in the near field of the source and its normal velocity is measured by a laser scanning vibrometer. Using a model equation considering acoustically induced vibration of the membrane, the original sound field radiated by the source is calculated and used for reconstruction of the normal source velocity. Preliminary theoretical results obtained in a mathematical model of the real situation are presented in this experiment.

5.2.1 Vibration of a thin square membrane

In Cartesian coordinates, the vibration of a rectangular thin membrane is described by the two-dimensional wave equation for a deflection ξ

$$\frac{\partial^2 \xi}{\partial x^2} + \frac{\partial^2 \xi}{\partial y^2} = \frac{1}{c_{\mathrm{M}}^2} \frac{\partial^2 \xi}{\partial t^2}, \tag{5.4}$$

where $c_{\mathrm{M}} = \sqrt{\nu / m_1}$ is the speed of a wave on the membrane, ν is tension (force per unit length) and m_1 is the mass per unit area [45]. The eigenfrequencies of the square membrane with a side a are given by

$$\omega_{mn} = \frac{\pi c_{\mathrm{M}}}{a} \sqrt{m^2 + n^2} \qquad m, n = 1, 2, \ldots \tag{5.5}$$

The characteristic functions fulfilling Eq. (5.4) are

$$\xi_{mn} = B_{mn} \sin \frac{m \pi x}{a} \sin \frac{n \pi y}{a}, \tag{5.6}$$

where B_{mn} are amplitudes of corresponding eigenfunctions. The modal impedance of the thin square membrane is

$$Z_{mn} = \frac{\rho h a^2}{4} (\omega_{mn}^2 - \omega^2), \tag{5.7}$$

where ρ and h are density and thickness of the membrane, respectively; ω is angular frequency.

5.2.2 Acoustically induced vibration

The acoustic pressure on the rigid planar surface (with no motion) is comprised of the incident pressure p_i (without the plate) and of the equal pressure due to the presence of the plate. This double pressure is usually called blocked pressure p_bl [46].

$$p_\mathrm{bl} = 2p_\mathrm{i}.$$

The total acoustic pressure in front of the real membrane that is acoustically induced (and hence radiates) is then the sum of the blocked pressure and the pressure radiated due to the vibration of the membrane. The blocked pressure defines the modal blocked force F_bl^{mn} on the plate surface as

$$F_\mathrm{bl}^{mn} = \int_S \xi_{mn}(\mathbf{r}_\mathrm{s}) p_\mathrm{bl}(\mathbf{r}_\mathrm{s}) dS, \tag{5.8}$$

where the vector $\mathbf{r}_s$ specifies the points on the surface. The modal impedance is defined as

$$Z_{mn} = \frac{F_\mathrm{bl}^{mn}}{v_{mn}} \tag{5.9}$$

where $v_{mn} = -\mathrm{j}\omega\xi_{mn}$ is modal velocity. The modal impedance is real for the mode excited at the resonance, otherwise it is complex.

5.2.3 Estimation of blocked pressure

We assume velocity distribution $v_\mathrm{n}(x, y)$ on the membrane (i.e. measured by a laser scanning vibrometer). The total acoustic pressure inducing this membrane vibration can be described using Eq. (5.4) as

$$\frac{\partial^2 \xi}{\partial x^2} + \frac{\partial^2 \xi}{\partial y^2} - \frac{1}{c_\mathrm{M}^2} \frac{\partial^2 \xi}{\partial t^2} = \frac{2p_\mathrm{i} + 2\rho c v_\mathrm{n}}{m_1}, \tag{5.10}$$

where c is the speed of a wave in the air. The incident pressure from Eq. (5.10) is

$$p_\mathrm{i} = \frac{\nu a}{2\mathrm{j}\omega} \Delta v_\mathrm{n} - \rho c v_\mathrm{n} - \frac{\mathrm{j}\omega m_1}{2} v_\mathrm{n}, \tag{5.11}$$

where Δ is the Laplace operator.

5.2.4 Simulation

The model source is represented by a baffled square plate with side $a_\mathrm{p} = 0,6\,\mathrm{m}$, thickness $h_\mathrm{p} = 2\,\mathrm{mm}$, density $\rho_\mathrm{p} = 7600\,\mathrm{kg.m^{-3}}$ (steel), Young's modulus

$E_\mathrm{p} = 210\,\mathrm{GPa}$ and Poisson's ratio $\nu_\mathrm{p} = 0,3$. Plate is excited by a point harmonic force of frequency f at position x_p, y_p.
The square membrane with side $a_\mathrm{m} = 0,6\,\mathrm{m}$ (same as the source), thickness $h_\mathrm{m} = 0,3\,\mathrm{mm}$ and density $\rho_\mathrm{m} = 4000\,\mathrm{kg.m}^{-3}$ is placed in the near field of the source at a distance $z_\mathrm{m} = 5\,\mathrm{cm}$.
In the first experiment, the source is excited by a point force of frequency $f = 500\,\mathrm{Hz}$ at position $x_p = 12,5\,\mathrm{cm}$, $y_p = -5\,\mathrm{cm}$. In the top of Fig. B.1, the normal velocity of the source is shown together with the pressure radiated by this source at a distance z_m and normal velocity induced on the membrane. At the bottom of Fig. B.1, the estimation of pressure incident to the membrane and reconstruction of the normal source velocity by SONAH is shown. The vibration of the source and the membrane was modeled with modal orders m and n up to 5. No additional noise is used in this case.
In Fig. B.2, the effect of additional noise in incident pressure to the reconstruction is illustrated. The relative error of reconstruction is computed in relation to source normal velocity. The number of points (reconstructed on the source surface) in which the relative error is less than the given percentage is plotted at the top of Fig. B.2. Noise level is the multiple of the mean incident pressure value $A_\mathrm{n}\bar{p}_i$. At the bottom of the figure, the reconstructions for three different A_n are shown.

5.2.5 Conclusions

The theoretical study of reconstruction of normal velocity on the source surface from the measurement of normal velocity on the auxiliary surface was the subject of this study. The auxiliary surface represented by a thin square membrane is situated in the near field of the source and is acoustically excited by its radiation. The relations between membrane vibration and incident pressure were described. On the model experiment, the reconstruction of normal source velocity was performed by SONAH. The influence of noise in incident pressure was illustrated.
This approach could be used in a situation where the laser scanning vibrometer measurement is complicated or impossible. The membrane is assumed not to affect the source vibration, which is an acceptable assumption for many types of acoustic sources.

5.3 Holographic reconstruction of an incident field assuming the spherical waves scattered by a rigid sphere

The study presented in [47] deals with the reconstruction of an acoustic field in the near-field around a rigid sphere using Near-field Acoustical Holography (NAH) based on an expansion in terms of the spherical harmonics. By employing the rigid sphere providing stable inversion of the propagation function one has to take into account the scattering effect that could significantly affect the total field around the sphere. This effect is commonly accounted for the separation of the incident and scattered field from the total measured field. In applications performing sound field reconstruction by NAH, the presence of source in the near-field of the sphere is to be expected. In this study, such a source in the near-field is considered and a method for determination of the source distance is examined. We consider the spherical waves scattered by a rigid spherical surface for the separation and subsequent reconstruction of the only incident field in this paper. The results are presented in a model simulation.

5.3.1 Model evaluation

Sound field reconstruction, as well as determination of the source distance, is presented using a model data set (without noise). In the following, a rigid sphere of radius $R = 0.15\,\mathrm{m}$ is considered. The point source of frequency $f = 300\,\mathrm{Hz}$ is placed on the positive x axis at a radius $r_s = 0.3\,\mathrm{m}$ from the coordinate origin. An array of order $N = 4$ is modeled (the number of sampling points is high enough to sample the data spatially without the aliasing effect). Thus, according to Eq. (4.32), the near-field of such an array for the above-mentioned frequency is r_{NF}=0.72 m. At the top of Fig. 3, the reconstruction of the acoustic intensity vector at the radius $r = 0.3\,\mathrm{m}$ is presented (depicted as arrows together with a colorful illustration of magnitude of the active intensity vector). In the pictures below, the incident and scattered field (magnitude of acoustic pressure) in the area $R \leq r \leq r_s$ are plotted on the cross-section perpendicular to the z axis at $z = 0\,\mathrm{m}$. The Fourier coefficients computed on the surface of an array are shown for both fields at the bottom of Fig. C.1. Determination of the source distance (using Eq. (4.38)) is shown up to $n = 3$ (note that coefficients of order $n + 1$ are needed) on the top of Fig. C.2. The middle picture demonstrates the behavior of this method for increasing array order (N=10). It can be seen that this method approaches the true value with increasing array order for noiseless data. However, bearing in mind that the Fourier coefficients decay

rapidly when $n > kR$ (see discussion in chapter 5 in [3]), the higher orders are the most contaminated by the measurement noise and the determination of source distance using these orders is inaccurate and unreliable. Therefore, the optimal orders according to the near-field condition and the coefficient decay condition have to be chosen. Relative to the fact that the above-mentioned conditions have no common intersection (because $r_s > R$), the several orders satisfying the near-field condition could be gradually used. An example of determination using noisy data (spatially uncorrelated white noise has been added to the sampled data) is shown for $N = 10$ at the bottom of Fig. C.2. The maximum level of the noise is set to 10 % of the mean value of simulated data. Note that no regularization is used. The green line shows the real distance while the red line stands for the actual value of kr_s (showing the behavior of approximations used to derive Eq. (4.38)). In Fig. C.3, a comparison is displayed of the spherical harmonics spectra of the field incident on an array, the field reconstructed at $r = r_s$ and the scattered field at the same radius as reconstruction. The strongest modes of the scattered field slightly exceed 10 % of the reconstructed field.

5.3.2 Conclusions

In this study, spherical Near-field Acoustical Holography is used for the reconstruction of the acoustic field around a rigid sphere. Both the reconstruction of the incident field alone and the computation of the scattered field in the volume between spherical array and sound source have been performed and presented for an appropriately situated point source on the corresponding cross-section. According to the values of the Fourier coefficients of the scattered field at the same position as reconstruction (the same position as the source, in this case), the scattered field would have only a weak influence on the source radiation. However, this effect has to be evaluated thoroughly depending on frequency, source distance and last but not least, in connection with the source dimensions and acoustical-mechanical parameters. The method for the source distance determination has been examined. It can be seen that this method is approaching the true value for increasing array order (under the near-field condition), nonetheless, recalling that Fourier coefficients decay rapidly when $n > kR$, the optimal selection of orders used for distance determination has to be carried out. This method could be useful in situations where the direct measurement of distance is impractical. However, it has to be tested in more complex situations where the other sources and/or reflections are significant.

5.4 Source Distance Determination Based on the Spherical Harmonics

The study presented in [48] deals with the processing of signals measured by a spherical microphone array, focusing on the utilization of near-field information of such an array. The processing, based on the spherical harmonics decomposition, is performed in order to investigate the radial-dependent spherical functions and extract their argument –distance to the source. Using the low-frequency approximation of these functions, the source distance is explicitly expressed. The source distance is also determined from the original equation (using no approximation) by comparing both sides of this equation. The applicability of both methods is first presented in the noise-less data simulation, then validated with data contaminated by the additive white noise of different signal-to-noise ratios. Finally, both methods are tested for real data measured by a rigid spherical microphone array of radius 0.15 m, consisting of 36 microphones for a point source represented by a small speaker. The possibility of determination of the source distance using low-order spherical harmonics is shown.

5.4.1 Model Validation

In this chapter, both methods are validated using the model data represented by a point source located at distance $r_s = 0.3\,\mathrm{m}$ from the origin (center of the sphere) for three different signal-to-noise ratios (SNR, modeled using the MATLAB function *awgn* as the ratio of signal power to noise power). For the purposes of this study, the array performance is evaluated according to the maximum order N while the aliasing effect is not considered – the model sphere of radius $a = 0.15\,\mathrm{m}$ is sampled in many more points than would be adequate for the given order. The Fourier coefficients are calculated according to Eq. (4.19) implemented by the Singular Value Decomposition (SVD). This approach is described in [34]. The determination for the order n, labeled in following pictures and tables, is performed using this order and the $(n+1)$ order (division of two adjacent mode strengths). A scheme of a typical experiment is depicted in Fig. D.1.

method	order									
	0	1	2	3	4	5	6	7	8	9
approx. r_s [m]	0.08	0.22	0.38	0.39	0.35	0.33	0.32	0.31	0.31	0.31
no approx. r_s [m]	0.30	0.30	0.30	0.30	0.30	0.30	0.30	0.30	0.30	0.30

Table 5.1: Noise-less data model simulation. Determined values of r_s [m]. True value is $r_s = 0.3\,\text{m}$ and $kr_s = 2.77$

5.4.2 Noise-less data

Firstly, the ideal situation with a model point source with $kr_s = 2.77$ ($f = 500\,\text{Hz}$) with no added noise is exemplary shown in Fig. D.2. The results of the approximation-based method are presented in the top part of this figure while the results of the no-approximation method are presented in the bottom part. The determination is performed up to $n = 10$ to show the convergent behavior (to the true source distance shown by the *green* horizontal line) of the approximation-based method; however, according to the above discussed validity of this method, the higher orders will not be useful in the case of noisy data. The *red* vertical line representing the actual value of kr_s is shown to evaluate the fulfillment of the approximation condition $kr_s << n$. In the bottom picture, the left-hand side of Eq. (4.35) is depicted for the given orders by solid curves, while the constant values of the right hand side are depicted by dashed lines. The mutual intersections are highlighted by the dots and actual distance is represented by the *black* vertical line. Of course, the same as before holds for higher orders, however, the determination is not limited at the lower orders. The determined distances are presented in Table 5.1 as well – the values in gray-marked cells do not satisfy the approximation condition and cannot be considered as usable results in general. Such an array capable of processing the data up to the 10th order would be, according to Eq. (4.32), able to utilize the near-field information up to the distance $r_{NF} = 1\,\text{m}$ at $f = 500\,\text{Hz}$. Nonetheless, it should be noted that the required number of microphones is related to the maximum order N of the spherical harmonics. For example, considering *nearly uniform sampling scheme* discussed in [23] the required number of microphones would be at best $(N+1)^2$, but in practice larger.

method	order					
	0	1	2	3	4	5
	SNR = 15 dB					
approx. r_s [m]	0.08	0.22	0.38	0.38	0.30	0.19
no appr. r_s [m]	0.30	0.30	0.30	0.29	0.27	0.19
	SNR = 10 dB					
approx. r_s [m]	0.08	0.22	0.37	0.40	0.23	0.16
no appr. r_s [m]	0.33	0.30	0.29	0.31	0.21	0.17
	SNR = 5 dB					
approx. r_s [m]	0.08	0.22	0.35	0.31	0.21	0.15
no appr. r_s [m]	0.36	0.29	0.28	0.25	0.20	0.16

Table 5.2: Noisy data model simulation. The average values of five realizations of the determination of r_s [m]. The true value is $r_s = 0.3$ m and $kr_s = 2.77$

5.4.3 Noisy data

The second model example shows the distance determination while the noiseless data were contaminated by the additive white noise of SNR=15, 10 and 5 dB. As has been already discussed, the noise mainly influences the higher orders, whose coefficients are comparable to the noise level. This finding applies for both methods, as clearly seen in Figure D.3. In this case, the determination becomes significantly erroneous for orders higher than 4. The bottom part of this figure shows the possibility of distance determination using Eq. (4.35) – the behavior of determination using lower orders will become clear from the following table. The determined distances can be seen in Table 5.2 for three different SNR. These values represent the average values of five realizations. The gray-marked values do not satisfy the approximation condition. The graphic representation of these values can also be seen in Figure D.4.

5.4.4 Real experiment

In this paragraph, both methods are validated using the data measured by the rigid sphere of radius $a = 0.15$ cm consisting of 36 microphones. Such an array is theoretically capable of operating up to the 5th order (of course, depending

method	order			
	0	1	2	3
approx. r_s [m]	0.13	0.31	0.38	0.14
no approx. r_s [m]	0.31	0.35	0.30	—

Table 5.3: Real measured data. Determined values of r_s [m], the true value is $r_s = 0.3\,\text{m}$ and $kr_s = 2.21$

on the sampling scheme), however, because of a slight aliasing effect, the maximum order $N = 4$ is assumed. Moreover, in the following example, the 4th order is significantly influenced by noise. A small speaker was used to represent a point-like source at a distance $r_s = 0.3\,\text{m}$ from the origin. The arrangement of the measurement is depicted in Figure D.5. In this experiment, the frequency $f = 400\,\text{Hz}$ has been chosen to reduce slightly the value of $kr_s = 2.22$ in order better to satisfy the approximation condition when using a relatively low maximum order. For both methods, the determined distances are stated in Table 5.3. Again, the values in the gray-marked cells do not satisfy the approximation condition. It can also be seen that the result for the highest order is strongly influenced by noise, which transpires by the unfeasible distance 0.14 m in case of the approximation-based method and no intersection of the curves in case of no-approximation method. Therefore, in this case, only the determination based on the low orders using Eq.(4.35) is usable.

5.4.5 Conclusions

This experiment was focused on the utilization of near-field information of data measured by the spherical microphone array in order to determine the distance to the origin of a spherical wave impinging on the array. The determination was based on the division of two adjacent overall spherical wave mode-strengths calculated using the Fourier coefficients of the spherical harmonics. Two methods, first using low-frequency approximation and the second using an original equation without approximation, are presented. The results of these methods as well as their comparison are presented with both model simulations (for different signal-to-noise ratios) and real measurement. The possibility of using low orders of spherical harmonics to determine the source distance has been shown. Concerning the design of an array while optimizing its near-field parameters, it is clear that both raising the maximum order and increasing the radius of the sphere will lead to the larger near-field extent.

The main advantages of the approximation-based method are its explicit formulation and therefore its ease of computation. However, regarding the opposite restrictions represented by the condition of approximation and the rapidly decaying behavior of the coefficients, it is always problematic to select the orders suitable for the source distance determination. On the other hand, the no-approximation method enables use of low orders, but the distance determination is more complicated and more computer-time-consuming.

This approach could find its application in situations in which the direct measurement of the distance to the source is impractical. Because of its functionality in the near-field, it could be connected with Near-field Acoustical Holography in order to determine the region of validity of the sound field reconstructions. The tracking of a point source moving in the near-field of an array, as well as the expansion of this approach to more complicated sources or multiple sources (e. g. by implementing sequential source separation/extraction methods), are the topics of the following research. It should be noted that when the assumption of spherical wavefront is not fulfilled exactly, the method will not provide correct results.

Chapter 6

Conclusions

This thesis deals with sound source(s) localization and sound field mapping. Its focus is specifically on nearfield acoustical holography. This method has been developed since the 1960s, yet it is not commonly used in practice nowadays mainly due to its relatively high measurement and computational demands and related cost requirements. Therefore, the method is still under research an development to make it accessible for common use.

The theoretical part of this thesis summarizes the physical and mathematical background necessary for discussed topic. It starts with a general description of the sound radiation introducing the Helmholtz and Rayleigh integral equations and discussing the areas of their validity. Then, the mathematical concept of regularization is reviewed and its necessity for a proper solution of an inverse problem constituted by the NAH is discussed. Finally, the theory of NAH is described while focusing on the planar and spherical coordinate systems reflecting the experiments presented in this thesis.

The experiments described in the thesis show particular parts of this very broad topic, specifically aiming to overcome several particular method difficulties. The first experiment tries to approximate more accurately the measured data while reducing the computational complexity of the SONAH and HELS using the combination of their wave models. The second experiment tries to overcome the requirement of a huge number of the measurement points necessary for high spatial resolution (especially for higher spatial frequencies) by employing a thin membrane whose acoustically induced vibrations are measured using the laser scanning vibrometer. The third experiment utilizes

the spherical microphone array to reconstruct the sound field – the most convenient approach for the most general measurement scenarios in which no prior assumption exists regarding the sound source(s). The last experiment focuses on the source distance estimation using the spherical harmonics providing the region of validity for the spherical NAH reconstruction. The conclusions related to individual experiments are stated in the corresponding sections of chapter 5.

Employing the spherical microphone array is a very promising approach for overcoming the difficulties related to the finite aperture relevant for a planar (as well as cylindrical) array. On the other hand, since the evanescent wave acquisition in the near-filed, the method operates the best if the aperture copies the source surface as much as possible – which is usually not the case for spherical microphone arrays. To capture the evanescent waves using the spherical array, the total number of microphones could be relatively large providing a sufficient array spatial resolution represented by the maximal spherical harmonics order. Assuming a stationary sound field, a number of techniques to decrease the total number of microphones have been proposed for mainly planar arrays - based on the motion in the time and synchronizing individual "snapshots" as well as the scanning measurement. This technique seems very promising for the spherical array (rotation on an array) and is an interesting topic for further research. Moreover, the design of such a rotating spherical array to provide maximal spatial resolution is another challenge. Utilization of thin membrane and a laser-scanning vibrometer could provide a much higher number of measurement points even in a shorter measurement time than scanning measurement using a microphone (or several microphones). This approach seems also very promising in connection with the advancing development of nanomaterials, however, there are still many questions to solve to be able to use it in practice (e.g. the mounting of the membrane or control of the stress in the membrane). In the processing part of the method, utilization of the wavelets (in arbitrary coordinate systems) could significantly improve the implementation performance as well as improve the accuracy of results in some scenarios. A connection of wavelets and sound field reconstruction using the nearfield acoustical holography seems (especially for a spherical array) a highly progressive and natural future research direction.

Relatively high measurements demands are the main reason of low practice usability of the NAH. Development of approaches to reduce these demands is, therefore, the most promising course of further research in order to make the NAH applicable in wider engineering tasks. These approaches could be based on the ideas mentioned in the previous paragraph, such as incorporating a rotating spherical array or a laser-scanning vibrometer and thin membrane, or developing the processing based on the wavelets. Another relatively new data acquisition technique called compressive sensing could provide a tool to reduce these demands.

Appendices

Appendix A

Results: Graphic presentation of section 5.1

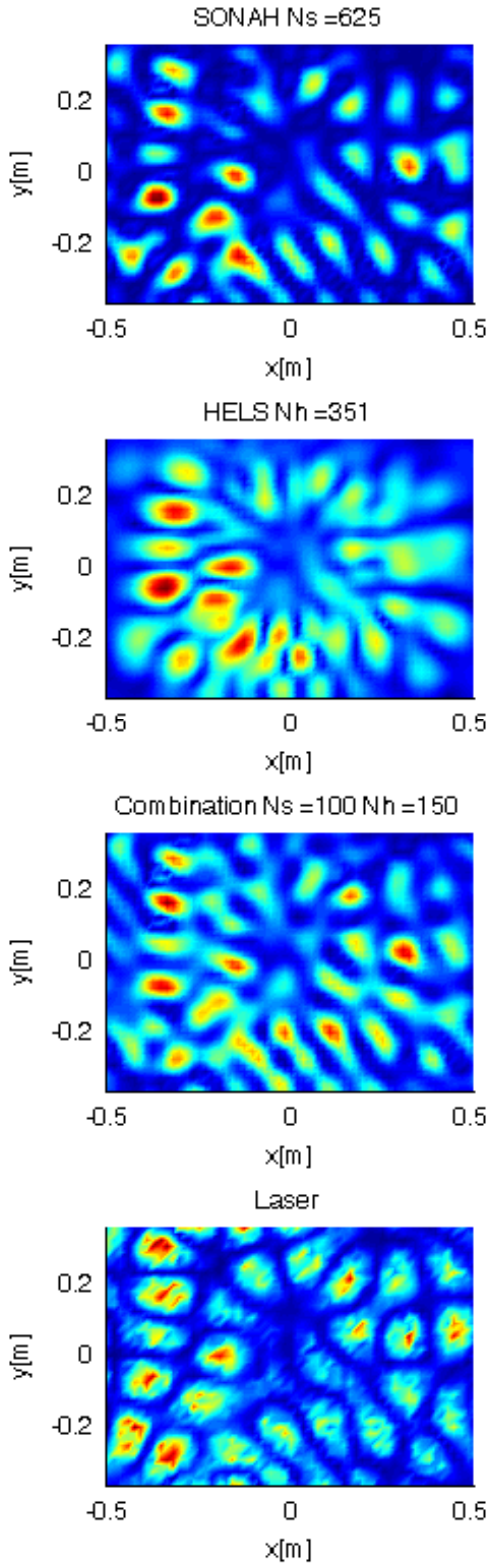

Figure A.1: Reconstruction of an acoustic pressure on the source plane for the band 508-512 Hz together with laser measurement

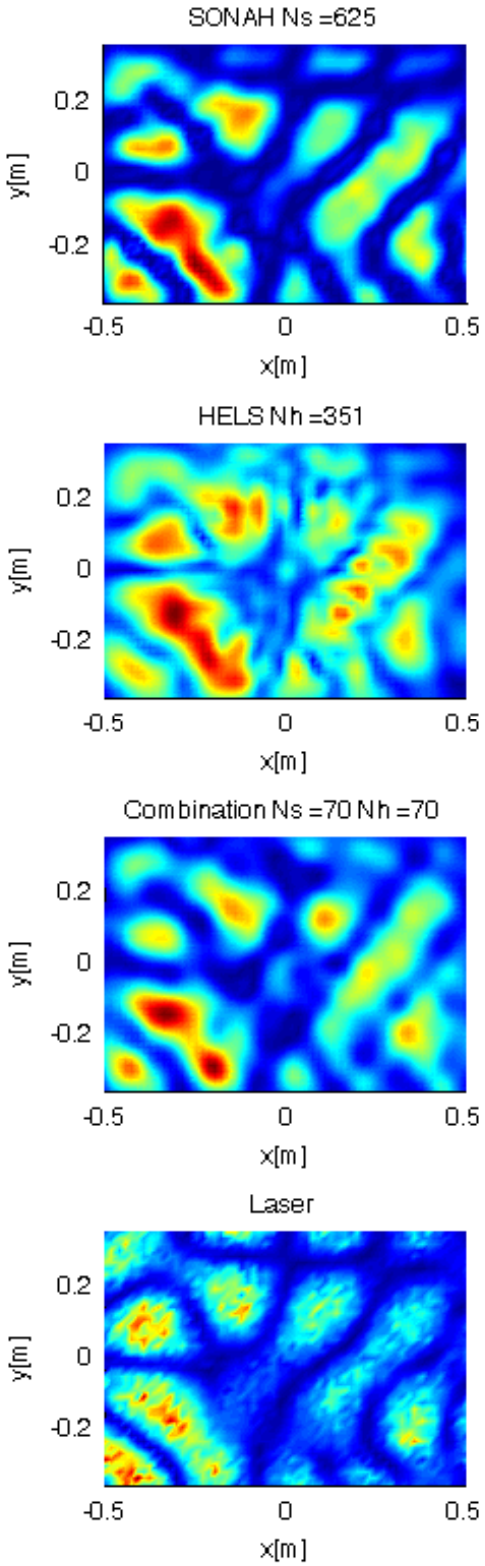

Figure A.2: Reconstruction of an acoustic pressure on the source plane for the band 176-178 Hz together with laser measurement

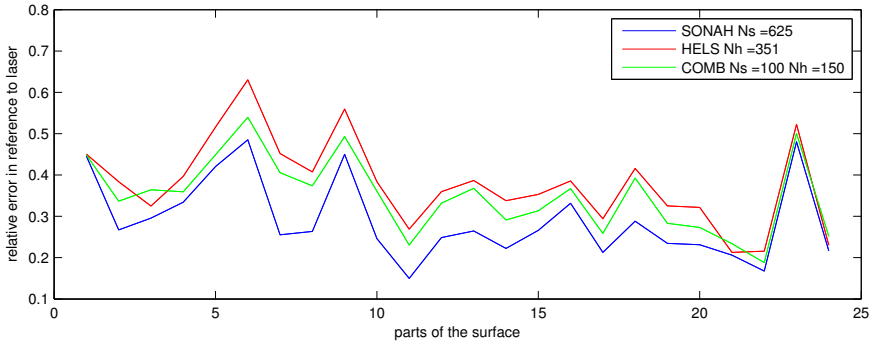

Figure A.3: Errors for the band 508-512 Hz

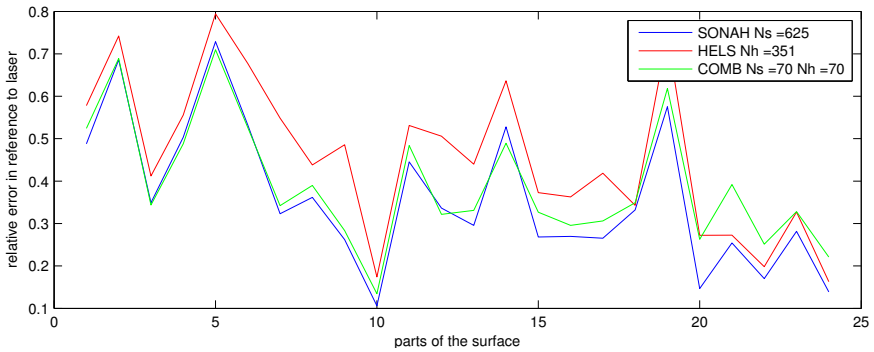

Figure A.4: Errors for the band 176-178 Hz

Appendix B

Results: Graphic presentation of section 5.2

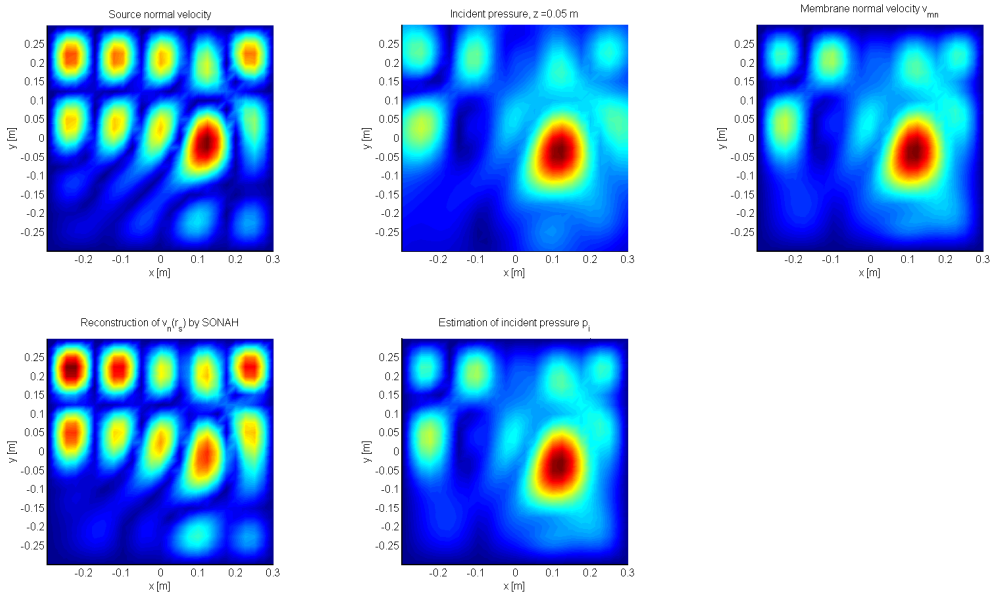

Figure B.1: Normal velocity of the source (top, left), pressure radiated by the souce at distance z_m (top, center), induced normal velocity on membrane (top, right), reconstruction of normal velocity on the suface (bottom, left), estimated incident pressure (bottom, center). Source excited by a point force at frequency $f = 500\,\mathrm{Hz}$ and position $x = 12,5\,\mathrm{cm}$, $y = 5\,\mathrm{cm}$

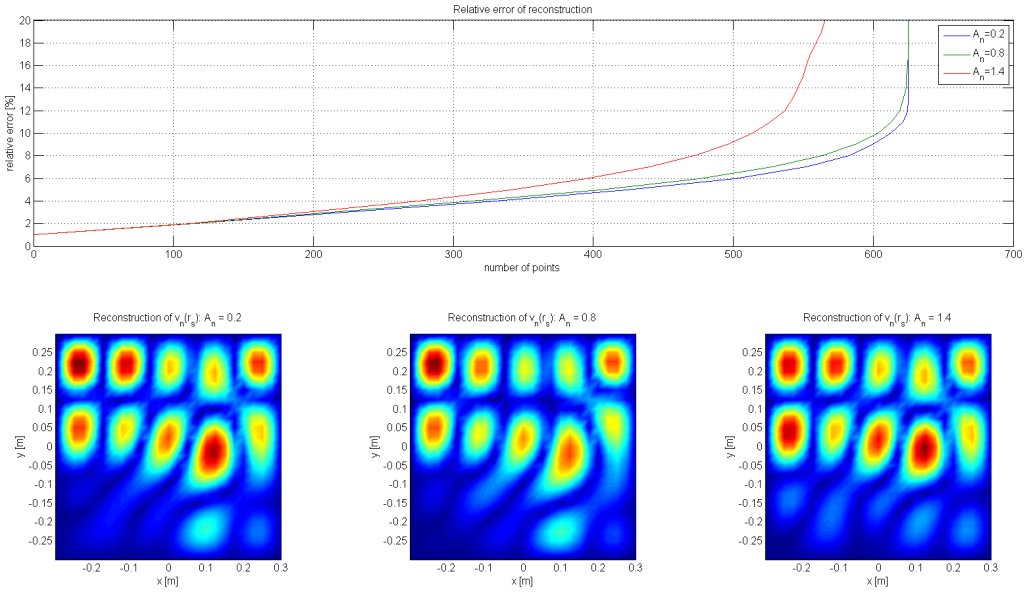

Figure B.2: Relative error of reconstruction in relation to source normal velocity (the number of points in which the relative error is less than given percentage) (top) – noise amplitude is $A_\mathrm{n}\bar{p}_\mathrm{i}$. Reconstruction of source normal velocity for $A_\mathrm{n} = 0.2$, $A_\mathrm{n} = 0.8$ and $A_\mathrm{n} = 1.4$ at bottom.

Appendix C

Results: Graphic presentation of section 5.3

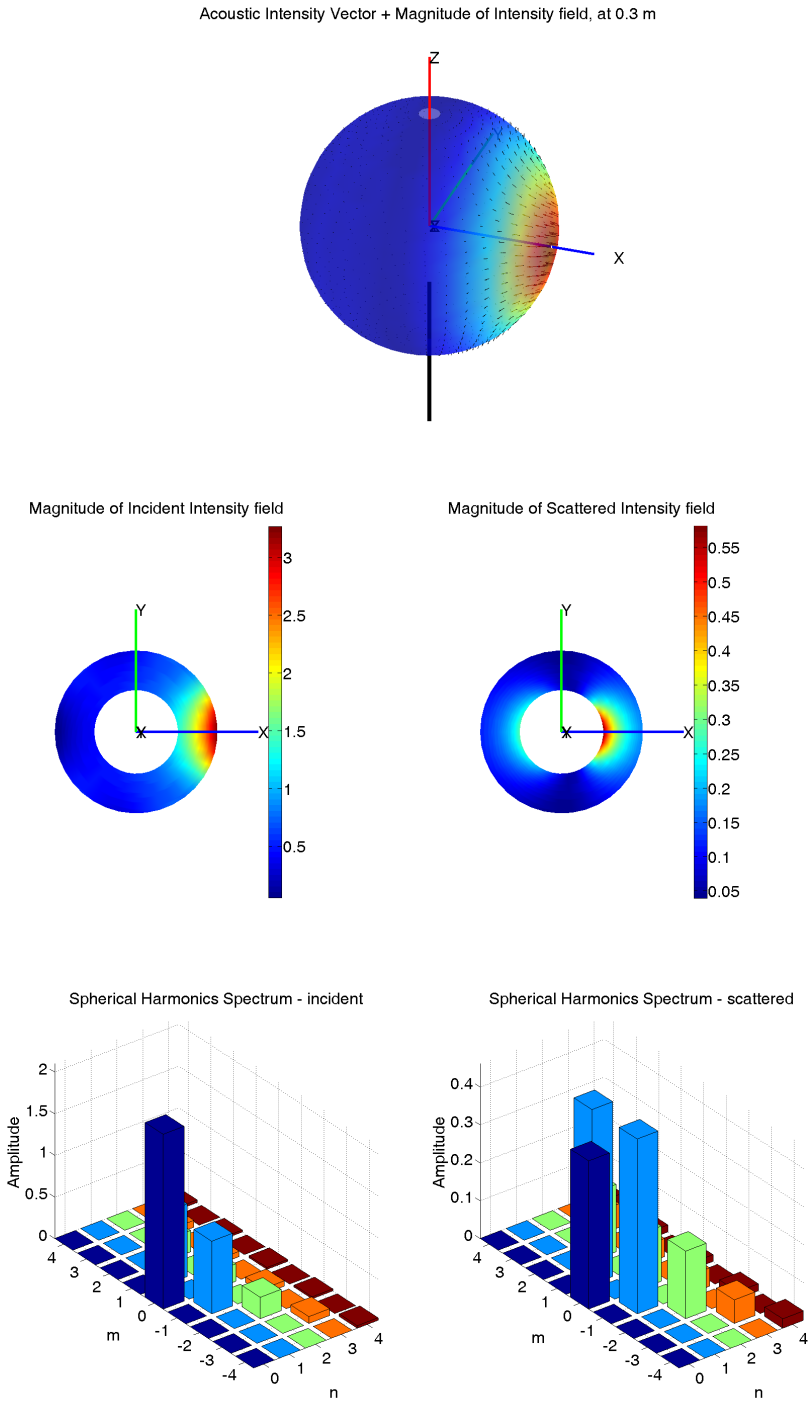

Figure C.1: Source at position ($\theta = \pi/2, \phi = 0, r_s = 0.3\,\mathrm{m}$), frequency $f = 300\,\mathrm{Hz}$. Top: Reconstruction of an active intensity vector at $r = r_s$. Middle: Magnitude of incident and scattered acoustic pressure on the cross-section perpendicular to z axis ($R \leq r \leq r_s$). Bottom: Fourier coefficients at $r = R$

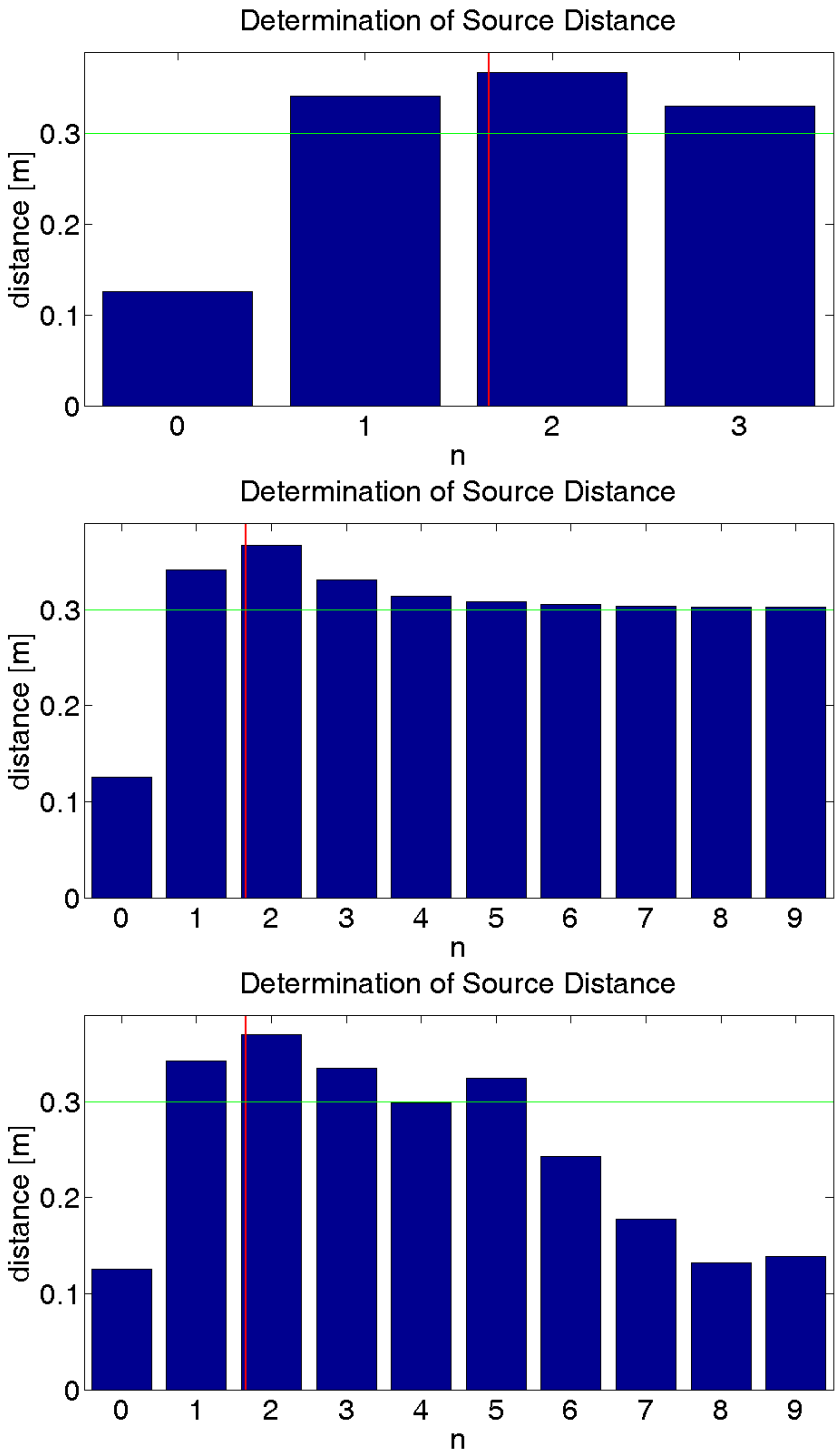

Figure C.2: Determination of source distance. Top: $N = 4$. Middle: $N = 10$. Bottom: $N = 10$, added noise. The green line shows the real distance (in this case $r_s = 0.3\,\mathrm{m}$) while the red line stands for the actual $kr_s = 1.66$

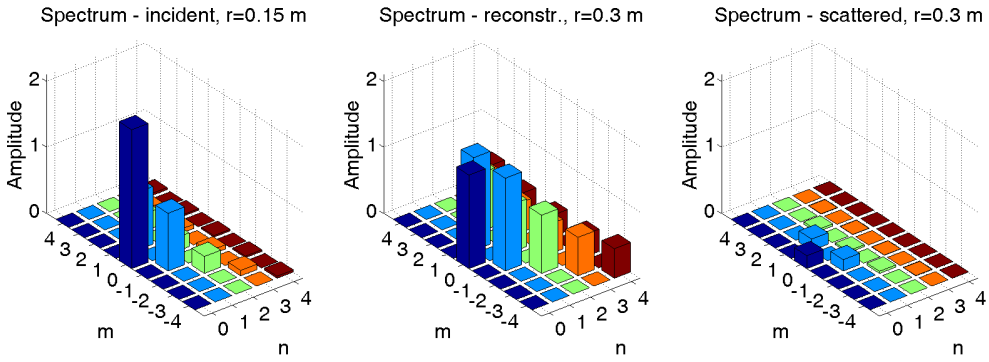

Figure C.3: Comparison of spherical harmonics spectrums for field incident on an array (left), reconstruction of this incident field at the source distance (middle) and the scattered field at the same radius of the reconstruction

Appendix D

Results: Graphic presentation of section 5.4

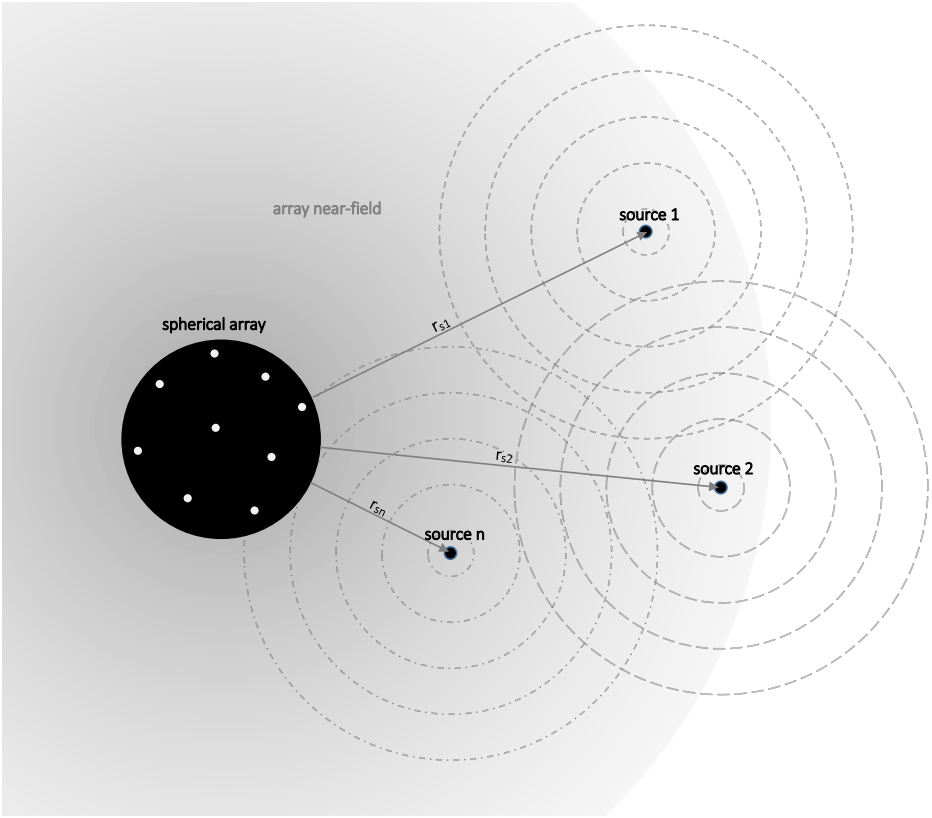

Figure D.1: Scheme of a typical experiment

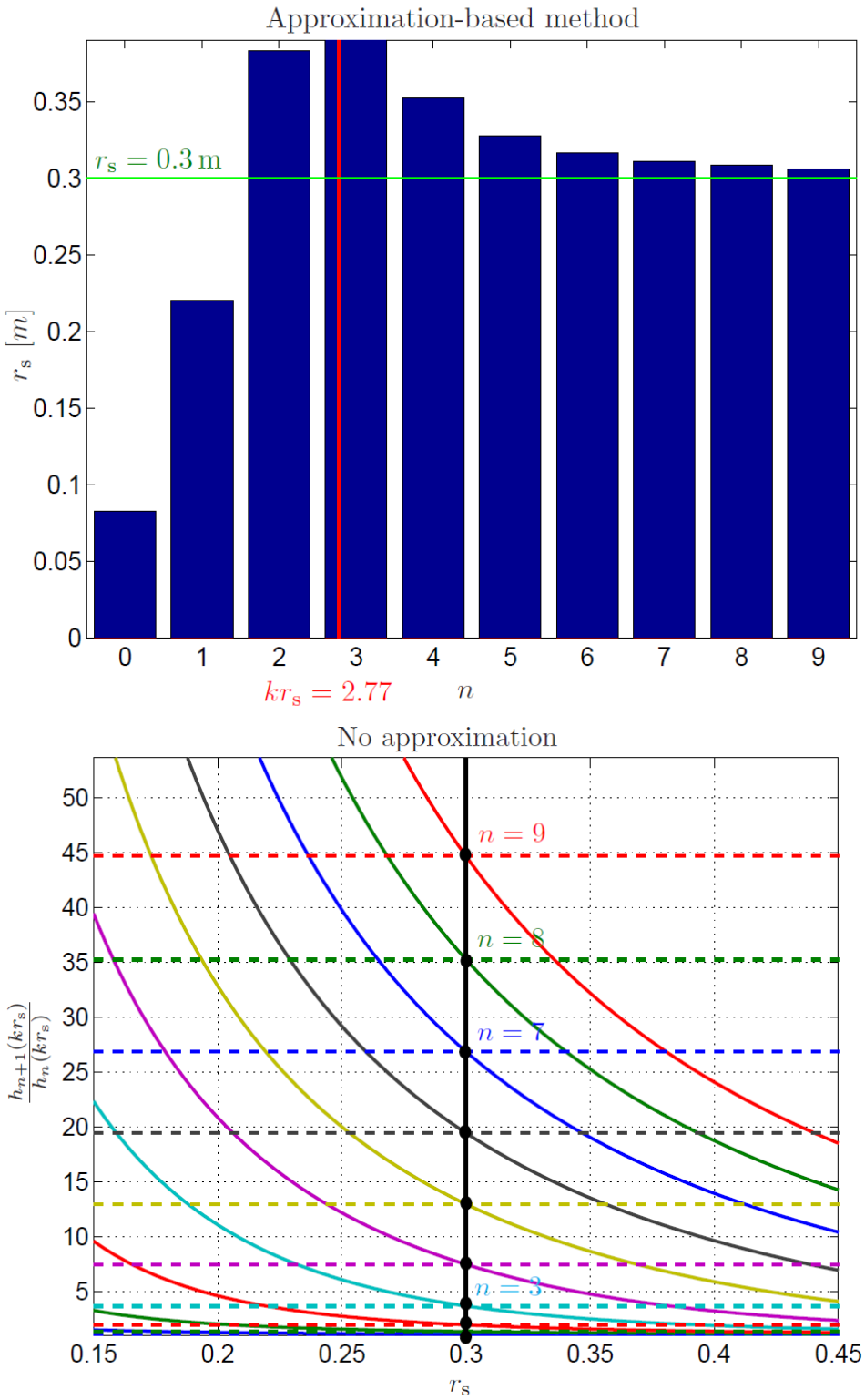

Figure D.2: Noise-less data model simulation. Top: approximation-based method. Bottom: no-approximation method. The determination for the order n, labeled in the pictures, is performed using this order and the $(n+1)$ order (division of two adjacent mode strengths)

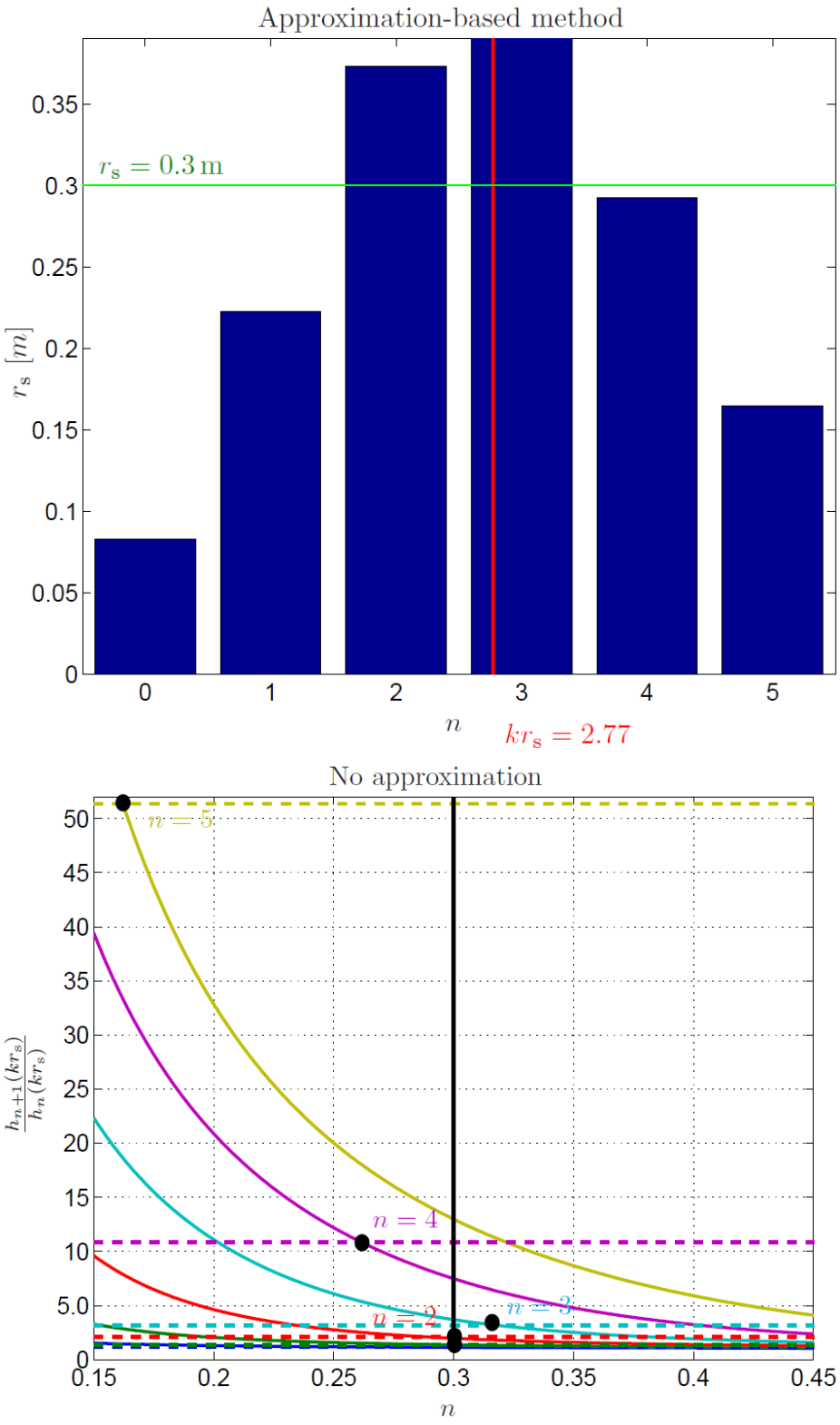

Figure D.3: Noisy data model simulation – SNR = 15 dB. Results of one realization. Top: approximation-based method. Bottom: no-approximation method. The determination for the order n, labeled in the pictures, is performed using this order and the $(n+1)$ order

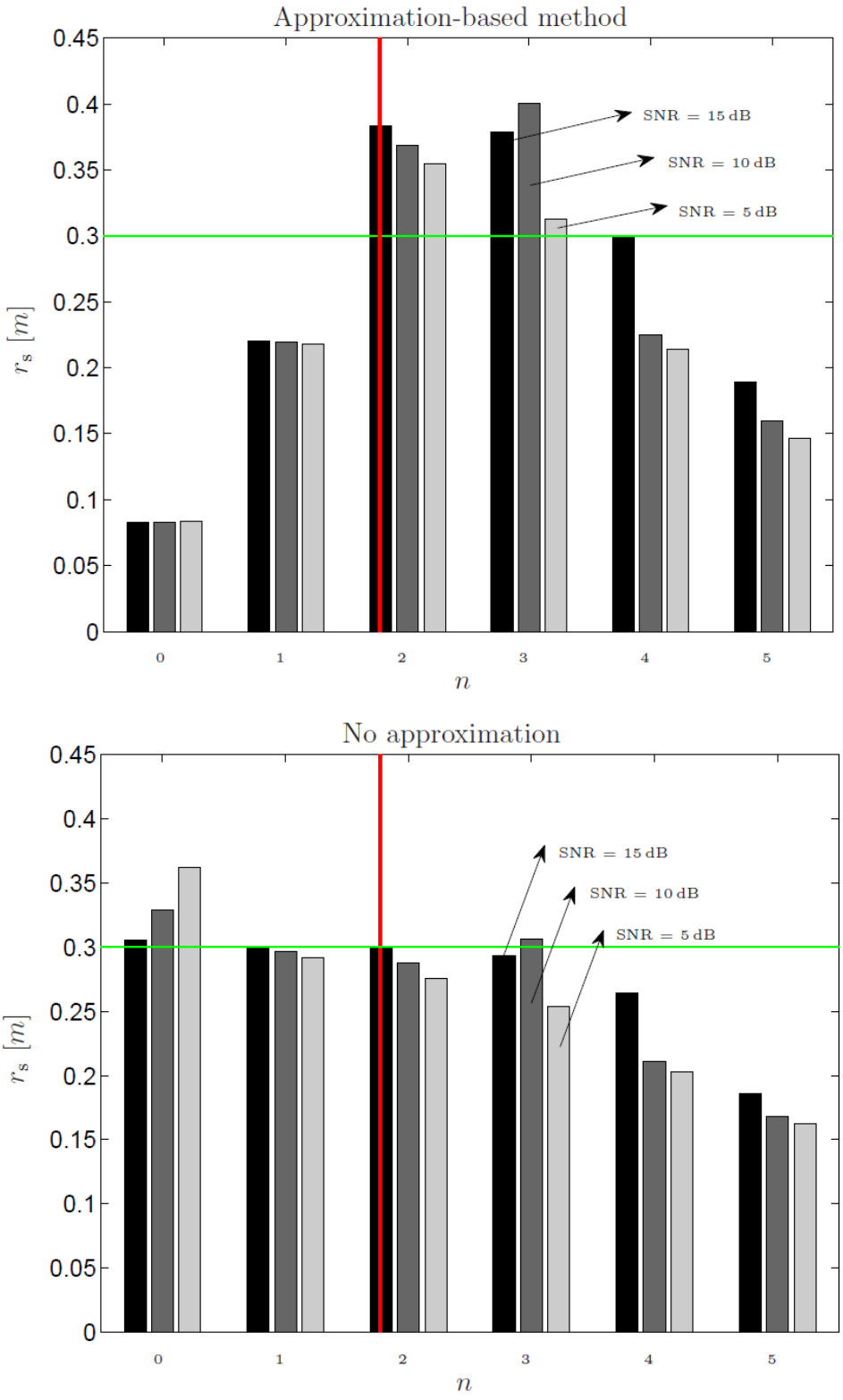

Figure D.4: Noisy data model simulation. Average values of five realizations of the determination of r_s [m]. Top: approximation-based method. Bottom: no-approximation method. The determination for the order n, labeled in the pictures, is performed using this order and the $(n+1)$ order (division of two adjacent mode strengths)

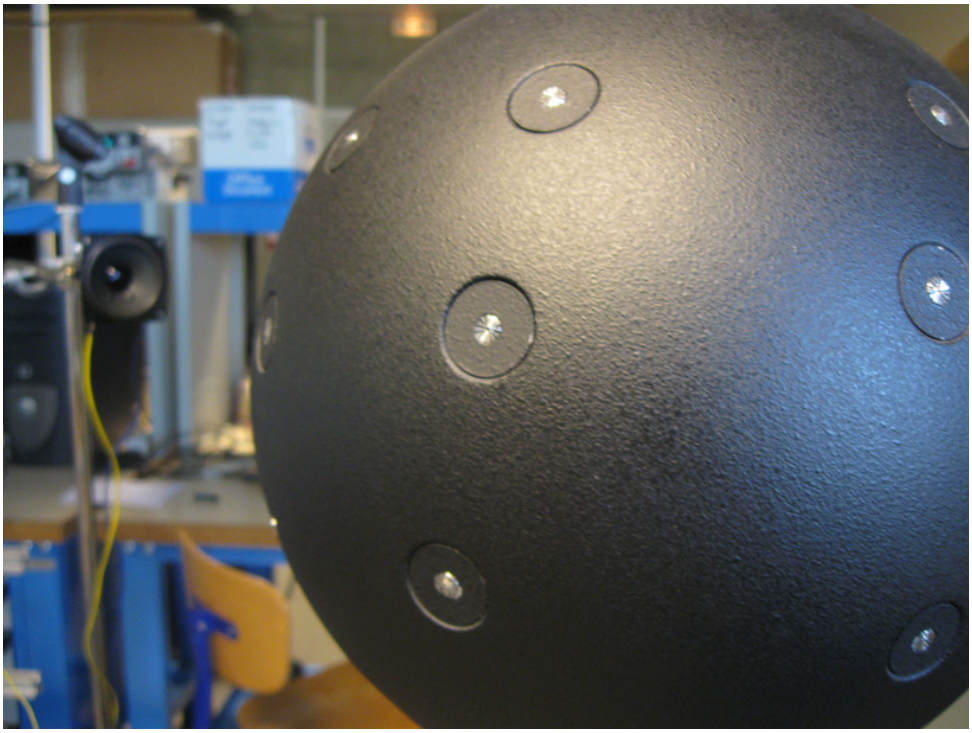

Figure D.5: Rigid sphere consisting of 36 microphones. The point-like source is represented by a small speaker placed at a distance 30 cm from the origin

Appendix E

Bibliography

[1] J. Billingsley and R. Kinns, "The acoustic telescope," *Journal of Sound and Vibration*, vol. 48(4), pp. 485–510, 1976.

[2] E. G. Williams, J. Maynard, and E. Skudrzyk, "Sound source reconstruction using a microphone array," *Journal of Acoustical Society of America*, vol. 68(4), pp. 340–344, 1980.

[3] E. G. Williams, J. Maynard, and Y. Lee, "Nearfield acoustic holography: I. theory of generalized holography and the development of nah," *Journal of Acoustical Society of America*, vol. 78(4), pp. 1395–1413, 1985.

[4] E. G. Williams, "Continuation of acoustic near-fields," *Journal of Acoustical Society of America*, vol. 113(3), pp. 1273–1281, 2003.

[5] T. Loyau, J.-C. Pascal, and P. Gaillard, "Broadband acoustic holography reconstruction from acoustic intensity measurements. i: Principle of the method," *Journal of Acoustical Society of America*, vol. 84, pp. 1744–1750, 1988.

[6] E. G. Williams, *Fourier Acoustics: Sound Radiation and Nearfield Acoustical Holography*. Academic Press, 1999.

[7] J. Hald, "Basic theory and properties of statistically optimized near-field acoustical holography," *Journal of Acoustical Society of America*, vol. 125(4), pp. 2105–2120, 2009.

[8] Z. Wang and S. F. Wu, "Helmholtz equation least-squares method for reconstructing the acoustic pressure field," *Journal of Acoustical Society of America*, vol. 102(4), 1997.

[9] S. F. Wu, "On reconstruction of acoustic pressure fields using the helmholtz equation least-squares method," *Journal of Acoustical Society of America*, vol. 107(5), pp. 2511–2522, 2000.

[10] J.-C. Pascal and J.-H. T. S. Paillasseur, "Patch near-field acoustic holography: Regularized extension and statistically optimized methods," *Journal of Acoustical Society of America*, vol. 126(3), pp. 1264–1268, 2009.

[11] E. G. Williams and B. H. Houston, "Fast fourier transform and singular value decomposition formulations for patch nearfield acoustical holography," *Journal of Acoustical Society of America*, vol. 114(3), pp. 1322–1333, 2003.

[12] Q. Leclère and B. Laulagnet, "Nearfield acoustic holography using a laser vibrometer and a light membrane," *Journal of Acoustical Society of America*, vol. 126(3), pp. 1245–1249, 2009.

[13] M. Bai, "Application of bem based acoustic holography to radiation analysis of sound sources with arbitrarily shaped surfaces," *Journal of Acoustical Society of America*, vol. 92(1), 1992.

[14] P. C. Hansen, *Discrete Inverse Problems: Insight and Algorithms*. SIAM, 2010.

[15] E. G. Williams, "Regularization methods for nearfield acoustical holography," *Journal of Acoustical Society of America*, vol. 110(4), pp. 1976–1988, 2001.

[16] F. Jacobsen and V. Jaud, "Statistically optimized near-field acoustical holography using an array of pressure-velocity probes," *Journal of Acoustical Society of America*, vol. 121(3), pp. 1550–1558, 2007.

[17] F. Jacobsen and Y. Liu, "Near field acoustic holography with particle velocity transducers," *Journal of Acoustical Society of America*, vol. 118(5), pp. 3139–3144, 2005.

[18] F. Jacobsen, V. Jaud, and C. Xinyi, "A comparison of statistically optimized near field acoustic holography using single layer pressure-velocity measurements and using double layer pressure measurements," *Journal of Acoustical Society of America*, vol. 123(4), pp. 1842–1845, 2008.

[19] J. Meyer and G. W. Elko, "A spherical microphone array for spatial sound recordings," *Journal of Acoustical Society of America*, vol. 111(5), pp. 2346–2346, 2002.

[20] T. D. Abhayapala and D. B. Ward, "Theory and design of high order sound field microphones using spherical microphone array," *Proc. IEEE Int. Conf. Acoust., Speech, Signal Processing. (ICASSP'02)*, vol. 2, pp. 1949–1952, 2002.

[21] J. Meyer and G. W. Elko, "A highly scalable spherical microphone array based on an orthonormal decomposition of the sound-field," *Proc. IEEE Int. Conf. Acoust., Speech, Signal Process. (ICASSP'02)*, vol. 2, pp. 1781–1784, 2002.

[22] M. Park and B. Rafaely, "Sound-field analysis by plane-wave decomposition using spherical microphone array," *Journal of Acoustical Society of America*, vol. 118(5), pp. 3094–3103, 2005.

[23] B. Rafaely, "Analysis and design of spherical microphone arrays," *IEEE Transaction on Speech and Audio Processing*, vol. 13(1), 2005.

[24] B. N. Gover, J. G. Ryan, and M. R. Stinson, "Microphone array measurement system for analysis omdirectional and spatial variations of sound fields," *Journal of Acoustical Society of America*, vol. 112(5), pp. 1980–1991, 2002.

[25] B. Rafaely, "Bessel nulls recovery in spherical microphone arrays for time-limited signals," *IEEE Transaction on Audio, Speech, and Language Processing*, vol. 19(8), November 2011.

[26] E. Fisher and B. Rafaely, "Near-field spherical microphone array processing with radial filtering," *IEEE Transaction on Speech and Audio Processing*, vol. 19(2), February 2011.

[27] E. B. Saff and A. B. J. Kuijlaars, "Distribution many points on a sphere," *New York: Springer-Verlag*, vol. 19(1), pp. 5–11, 1997.

[28] V. Lebedev, "Quadrature on a sphere," *Computational Mathematics and Mathematical Physics*, vol. 16, pp. 10–24, 1976.

[29] J. D. McEwen and Y. Wiaux, "A novel sampling theorem on the sphere," *IEEE Transactions on Signal Processing*, vol. 59(12), December 2011.

[30] I. B. Hagai, F. M. Fazi, and B. Rafaely, "Generalized sampling expansion for functions on the sphere," *IEEE Transactions on Signal Processing*, vol. 60(11), November 2012.

[31] B. Rafaely, B. Weiss, and E. Bachmat, "Spatial aliasing in spherical microphone arrays," *IEEE Transactions on Signal Processing*, vol. 55(3), December 2007.

[32] D. L. Alon and B. Rafaely, "Spherical microphone array with optimal aliasing cancellation," *IEEE 27th Convention of Electrical and Electronics Engineers in Israel*, 2012.

[33] E. G. Williams, N. Valdivia, P. C. Herdic, and J. Klos, "Volumetric acoustic vector intensity imager," *Journal of Acoustical Society of America*, vol. 120(4), pp. 1887–1897, October 2006.

[34] E. G. Williams and K. Takashima, "Vector intensity reconstructions in a volume surrounding a rigid spherical microphone array," *Journal of Acoustical Society of America*, vol. 127(2), pp. 773–783, February 2010.

[35] F. Jacobsen, G. Moreno-Pescador, and E. Fernandez-Grande, "Nearfield acoustic holography with microphones on a rigid sphere," *Journal of Acoustical Society of America*, vol. 129(6), pp. 3461–3464, June 2011.

[36] T. Szpruch and B. Rafaely, "Estimation of room impulse-response parameters using low-order microphone array," *IEEE 27th Convention of Electrical and Electronics Engineers in Israel*, 2012.

[37] G. H. Golub and C. F. V. Loan, *Matrix Computations (3rd ed.)*. Johns Hopkins, 1996.

[38] G. Strang, *Introduction to Linear Algebra (5th ed.)*. Wellesley-Cambridge Press, 2016.

[39] G. H. Golub, M. Heath, and G.Wahba, "Generalized cross-validation as a method for choosing a good ridge parameter," *Technometrics*, vol. 21, pp. 215–223, 1979.

[40] P. A. Nelson and S. H. Yoon, "Estimation of acoustic source strength by inverse methods: Part i, conditioning of the inverse problem," *Journal of Sound and Vibration*, vol. 233, pp. 643–668, 2000.

[41] S. H. Yoon and P. A. Nelson, "Estimation of acoustic source strength by inverse methods: Part ii, experimental investigation of methods for choosing regularization parameters," *Journal of Sound and Vibration*, vol. 233, pp. 669–705, 2000.

[42] R. Steiner and J. Hald, "Near-field acoustical holography without the errors and limitations caused by the use of spatial dft," *Int. J. Acoust. Vib.*, vol. 6, pp. 83–89, 2001.

[43] A. Koutný, P.Švec, and O. Jiříček, "Near-field acoustic holography based on combined elementary wave model," in *Forum Acusticum*, 2011. Aalborg, Denmark.

[44] A. Koutný, P. Švec, O. Jiříček, and M. Brothánek, "Reconstruction of normal surface velocity from measurement of acoustically induced vibration of a thin membrane," in *Euronoise*, 2012. Prague, Czech Republic.

[45] F. Fahy, *Sound and structural vibration. 2nd edition.* Elsevier, 2006.

[46] Z. Škvor, *Akustika a elektroakustika.* Academia, 2001.

[47] A. Koutný, O. Jiříček, and J.-H. Thomas, "Holographic reconstruction of an incident field assuming the spherical waves scattered by a rigid sphere," in *Internoise*, 2013. Innsbruck, Austria.

[48] A. Koutny, O. Jiříček, J.-H. Thomas, and M. Brothánek, "Source distance determination based on the spherical harmonics," *Mechanical Systems and Signal Processing*, vol. 85, pp. 993–1004, 2017.

Appendix F

Author's Publications

Related Publications

Impact journal articles:

- Koutný, A., Jiříček, O., Thomas, J.-H., Brothánek, M., *Source distance determination based on the spherical harmonics*, Mechanical Systems and Signal Processing, Vol. 85, p. 993-1004, February 2017
  - Impact Factor: 4.116
  - *All the authors contributed equally to the publication.*

Conference papers:

- Koutný, A., Jiříček, O., Thomas J.-H., *Holographic reconstruction of an incident field assuming the spherical waves scattered by a rigid sphere*, Inter-noise 2013, Innsbruck, Austria
  - *All the authors contributed equally to the publication.*

- Koutný, A., Švec, P., Jiříček, O., Brothánek, M., *Reconstruction of normal surface velocity from measurement of acoustically induced vibration of a thin membrane*, Euronoise 2012, Prague, Czech Republic
  - *All the authors contributed equally to the publication.*

- Koutný, A., Švec, P., Jiříček, O., *Near-field Acoustic Holography Based on Combined Elementary Wave Model*, 6th Forum Acusticum, June-July 2011, Aalborg, Denmark
  - *All the authors contributed equally to the publication.*
- Koutný, A., Švec, P., Jiříček, O., *Comparison of near-field acoustic holography regularization methods*, 1st EAA - EuroRegio, September 2010, Ljubljana, Slovenia
  - *All the authors contributed equally to the publication.*
- Koutný, A. - Švec, P.: *Porovnání regularizačních metod v akustické holografii a volba optimálních parametrů* (*Comparison of near-field acoustic holography regularization methods and methods for optimal regularization parameters choice*). In 80. akustický seminář. Praha: Česká akustická společnost, 2010, s. 35-43. ISBN 978-80-01-04547-3.
  - *All the authors contributed equally to the publication.*
- Koutný, A. - Jiříček, O. - Švec, P.: *Intenzitní p-u sonda pro měření akustické impedance* (*Acoustic intensity p-u probe for acoustic impedance measurement*). In Sborník 79. akustického semináře. Praha: Česká akustická společnost, 2009, s. 5-16. ISBN 978-80-01-04427-8.
  - *All the authors contributed equally to the publication.*

Other Publications:

Conference papers:

- Koutný, A., Pelant M., *Multi-channel degarbling method for SSR replies*, 18th International Radar Symposium (IRS), p. 1-11, June 2017
  - *All the authors contributed equally to the publication.*